RESEARCH ARTICLE

Frequency Selective Hybrid Beamforming and Optimal Power Loading for Multiuser Millimeter Wave Cognitive Radio Networks

INDRANIL CHATTERJEE[iD], **JITENDRA SINGH**[iD], (Member, IEEE),
SURAJ SRIVASTAVA[iD], (Member, IEEE),
AND ADITYA K. JAGANNATHAM[iD], (Senior Member, IEEE)

Department of Electrical Engineering, Indian Institute of Technology Kanpur, Kanpur 208016, India

Corresponding author: Indranil Chatterjee (indrac@iitk.ac.in)

ABSTRACT In this work, frequency selective hybrid precoders and combiners are designed for a millimeter wave (mmWave) multiuser (MU) multiple-input-multiple-output (MIMO) downlink underlay cognitive radio network (CRN) utilizing multiple radio frequency (RF) chains and uniform rectangular planar arrays (URPAs) both at the CR base station (CBS) and the secondary users (SUs). The proposed designs maximize the downlink spectral efficiency (SE) of the secondary users, while keeping the interference introduced to the primary user within a prescribed threshold. In the first phase, considering only the channel knowledge at each subcarrier, a novel blind hybrid MMSE-RC (minimum mean squared error-receiver combiner) design is determined using the modified simultaneous orthogonal matching pursuit (MSOMP). Further, employing feedback for each SU's effective channel, a two-stage decoupled strategy is developed for hybrid transmit precoder (TPC) design, wherein the RF and stage-1 BB-TPC are designed in the first step relying on a capacity-optimal fully digital (FD)-TPC approximation problem followed by the stage-2 BB-TPC design using a low-complexity ZF approach with the goal of mitigating the MUI. Towards this, a novel Modified Alternating Minimization-Zeroforcing (MAM-ZF) algorithm is proposed to compute the hybrid-TPC weights. Furthermore, a low complexity alternating minimization-zeroforcing (LAM-ZF)-based precoding algorithm is also proposed towards the same. Finally, a per-subcarrier optimal power loading solution is derived in closed-form with the objective of maximizing the sum SE while satisfying the interference and transmit power budget limitations. Our simulation findings show that the proposed schemes outperform other state-of-the-art techniques and achieve a spectral efficiency comparable to that achieved by fully-digital beamforming, while requiring a significantly fewer number of RF chains.

INDEX TERMS mmWave, cognitive radio networks, frequency selective, hybrid beamforming, multi-user, MIMO, OFDM, sparse reconstruction.

I. INTRODUCTION

The ever increasing density of connected devices has necessitated the exploration of new frequency resources to address the imminent radio spectrum crunch. Communication in the millimeter wave (mmWave) regime, which uses the wide 30-300 GHz band, has been embraced by the wireless industry to relieve spectral congestion by harnessing the vast blocks of spectrum available in this frequency range [1], [2]. On the other hand, measurement campaigns have led to the conclusion that traditional fixed license-based static spectrum allocation policies have resulted in a remarkably low efficiency of spectrum utilization [3]. In order to address this problem, researchers, and policy regulators have proposed dynamic spectrum allocation policies that allow spectrum sharing towards improved spectrum utilization. Cognitive radio networks (CRN), which support flexible policies that allow secondary users (SUs) to use licensed spectrum, while not causing adverse interference to the primary users (PUs), have emerged as a promising solution

for dynamic spectrum access [4]. Furthermore, the underlay mode, in which the SUs and PUs coexist in the same band, with the SU transmit power regulated to meet the interference constraints imposed by the PU, is the most viable mode of secondary access as it does not require a sophisticated spectrum sensing mechanism [5]. Thus, the high-frequency mmWave band, coupled with the underlay CRN-based dynamic spectrum allocation framework, is crucial to expanding as well as maximizing the effectiveness of spectrum utilization in beyond 5G (B5G) wireless networks. In addition, the flexibility of cognitive radio technology, combined with the advantages of mmWave frequencies, opens up new applications across various domains, including wireless backhaul, intelligent transportation systems, and Internet of Things (IoT), among others. It must also be noted that multi-input multi-output (MIMO) technology, which can enable the formation of highly directed beams, is critical toward overcoming the significant path and the penetration losses that are an intrinsic feature of mmWave propagation. Interestingly, the remarkably short wavelength in the mmWave regime allows the packing of a large number of antennas in devices of relatively small form factors, thus paving the way for seamless implementation of MIMO transceivers [6]. In addition, the fully-digital (FD) transmit precoders (TPCs) and receiver combiners (RCs) employed in a conventional MIMO system are inefficient for the mmWave communication. This is due to the fact that FD TPCs/RCs require a separate radio frequency (RF) chain for each antenna, which consume a substantial amount of energy. This accounts for approximately 70% of the total energy consumption at mmWave frequencies [7]. Furthermore, the cost of RF components operating at such high frequencies is considerably high, which increases the overall system cost. The hybrid MIMO design advocated in path-breaking works such as [8] and [9], which performs signal processing in the analog and digital domains, has been proven effective in addressing this challenge since it can operate with a significantly reduced number of RF chains compared to the number of antennas. Orthogonal frequency division multiplexing (OFDM) has been widely recognized in the literature as being ideally suited for CR systems, due to its ability to enable ultra-high data rates over a wide band. In such a mmWave MIMO OFDM CRN, the construction of an efficient TPC/RC is a formidable challenge because of the hardware limitations, paired with the PUs' stringent interference constraints. A concise overview of the relevant research works and their contributions to this field is discussed next.

A. LITERATURE REVIEW

The research papers [10], [11], [12], [13], [14], [15], [16] have shown that mmWave technology can be enormously advantageous for spectrum sharing due to its capability for highly directed beamforming at mmWave frequencies, which can effectively mitigate interference while simultaneously enhancing the user rate. Specifically, Gupta et al. in [10]

analytically prove that license sharing among operators in mmWave cellular systems enhances the system performance by boosting the per-user rate when the antennas have narrow beams. Soon afterwards, Rebato et al. in [11] have shown that, compared to the exclusive licence model, the performance gains reaped via spectrum sharing might be as high as 130%. The most recent work [16] studied the performance of spectrum sharing systems operating in the 26 GHz and 70 GHz bands, with ideal as well as non-ideal beamforming considering a real environment. Their research shows that a spectrum-sharing network may attain a total capacity that is two to three times higher than that of an exclusive licensing network. However, beamforming errors, poor interference mitigation mechanisms make it unlikely to offer any performance benefits in a dense shared network, especially for users with low SINR. Li et al., in their treatise in [13], developed an optimization framework based on joint beamforming, coordination, and base station (BS) association to maximize the throughput and fairness of the users in a mmWave shared spectrum network, followed by analyzing the efficacy of coordination and base station (BS) association towards interference management. The authors in [17] suggested a solution for interference management in underlay spectrum sharing and demonstrate its efficacy through simulation findings. Several existing studies [8], [9], [18], [19], [20], [21], [22], [23], have presented optimal hybrid TPC/RC designs for a frequency selective mmWave MIMO channel. Specifically, Alkhateeb and Heath in [8] investigated a codebook design algorithm for frequency selective hybrid TPC design, considering a limited feedback wideband mmWave MIMO system. In [24], Sohrabi and Yu, propose a novel design algorithm for hybrid beamforming in mmWave point-to-point (P2P)-MIMO and multiuser multiple-input-single-output (MU-MISO) systems. Their study shows that the minimum number of RF chains needed in a hybrid architecture to realize any fully digital beamforming matrix is equal to double the number of active data streams. Following this, in [9], the same work has been extended to mmWave P2P-MIMO-OFDM and MU-MISO-OFDM systems. Obtaining the CSI for each subcarrier in a wideband mmWave MIMO system is burdensome. To tackle this issue, the authors in [21] developed practical hybrid beamforming techniques based on statistical channel information, in which columns of both the BB and RF-TPC are picked from their respective codebooks using a low-complexity search algorithm. The most recent work in [23] presented a joint RF-TPC/RC design procedure employing the constrained Tucker2 tensor decomposition technique to suppress the MUI and enhance the effective BB channel in an MU frequency-selective mmWave MIMO system.

The aforementioned papers and references constitute a substantial body of research on spectrum sharing in mmWave networks and hybrid TPC/RC design in mmWave MIMO-OFDM systems. However, the design of hybrid TPC/RC subject to interference constraints, considering

TABLE 1. Contrasting our contribution on mmWave MSU-MIMO-OFDM CR to the existing literature.

	[16]	[24]	[28]	[8]	[20]	[9]	[14]	[22]	[25]	[29]	[21]	[30]	Proposed Work
mmWave MIMO system	x	✓	✓	✓	✓	✓	✓	✓	✓	✓	✓	✓	✓
Frequency selective channel	x	x	x	✓	✓	✓	x	x	x	x	✓	x	✓
Muli-user	✓	x	✓	x	✓	x	✓	✓	x	✓	x	✓	✓
Multi RF chain user	x	✓	x	✓	x	✓	x	x	✓	✓	✓	✓	✓
Underlay CRN	✓	x	✓	x	x	x	✓	x	✓	✓	x	✓	✓
Hybrid TPC	✓	✓	✓	✓	✓	✓	✓	✓	✓	✓	✓	✓	✓
Hybrid MMSE-RC	x	✓	x	✓	x	✓	✓	✓	✓	✓	✓	✓	✓
MUI cancelling TPC	✓	x	✓	x	✓	x	x	x	x	x	x	✓	✓
Optimal power loading	x	x	x	x	x	x	x	x	x	x	x	✓	✓

multiple users with several RF chains and antennas, has been scarcely studied. In [25], a hybrid TPC/RC design is proposed for a single user MIMO-CRN based on the SE maximization criterion. The work in [26] investigates hybrid beamforming for spectrum sharing backhaul networks. Authors in [27] and [28] investigated hybrid TPC/RC design subject to maximizing the minimum secrecy rate of all the secondary users under practical constraints. The recent work in [29] extended the work in [25] considering both uplink and downlink mmWave MU-MIMO underlay CRNs, however, with complete channel state information (CSI). As a further advance, our work in [30] proposed a hybrid TPC/RC design procedure coupled with an optimal power allocation strategy to maximise the SE relying on limited feedback. To the best of our knowledge, the problem of frequency selective hybrid TPC/RC design for a MSU-MIMO-OFDM CRN has not been addressed yet in the current literature, which forms the focus of this work. The proposed technique can support multiple users with multiple RF chains and optimally allocate power based on the available channel state information (CSI), for a given transmit power budget, while meeting the interference power constraints imposed by the PU. The novel contributions of this study are itemized next and a comparison to those of the literature cited above is presented in Table 1.

B. CONTRIBUTIONS OF THIS WORK

- A hybrid TPC/RC design technique is proposed that maximizes the SE with interference and transmit power constraints as well as hardware limitations for a down-link wideband mmWave-MIMO underlay CRN. The optimization problem is developed considering multiple SUs and a single PU, each equipped with a uniform rectangular planar array (URPA) and multiple RF chains. The optimization problem above is decomposed into two sub-optimization problems in order to tackle the non-convex nature of the original problem.
- Initially, the optimal *blind* hybrid MMSE-RC design problem is solved for each SU, considering the optimal per-subcarrier FD-TPC with blind equal power loading for each stream at the CBS. The hybrid combiner design paradigm is formulated as a multiple measurement vector-based sparse signal recovery problem and solved using a modified simultaneous orthogonal matching pursuit (MSOMP) technique.
- Next, the corresponding sum SE maximization problem with all the constraints mentioned above is once

again formulated and solved considering the feedback knowledge of each SU's effective channel matrix, which consists of the blind hybrid MMSE-RC and channel for each subcarrier. An optimized two-stage hybrid TPC design procedure is then described, wherein the RF and stage-1 BB-TPC are designed in the first step, relying on a capacity-optimal FD-TPC approximation problem. A novel modified alternating minimization (MAM) algorithm is developed to address the stage-1 TPC design. Moreover, a modification is also proposed for the TPC design algorithm presented in [31], which has been shown to have lower complexity and faster convergence. Stage-2 aims to mitigate the MUI by designing the BB-TPC using a low-complexity ZF approach.
- Finally, employing the RF, stage-1, and stage-2 TPCs, an optimal power loading solution is obtained in closed-form to maximize the overall SE while adhering to the interference and power constraints.

C. ORGANIZATION

The remaining sections of this work are structured as follows. Section II presents the multiple SU (MSU)-MIMO-OFDM downlink CRN model followed by the discussion pertaining to the mmWave MIMO-OFDM channel and formulation of the hybrid transceiver design optimization problem. Section III deals with the blind hybrid-MMSE RC design procedure. In section IV we demonstrate the two-stage hybrid TPC design followed by the optimal power loading strategy. Section VI showcases our simulation findings, and finally, conclusions are drawn in Section VII.

D. NOTATION

We use the following notation throughout this paper: Bold lowercase and uppercase letters indicate vectors and matrices, whereas lowercase letters signify scalar quantities. The inverse, Hermitian, (p, q)th element, pth column of a matrix $\mathbf{B}$ are denoted by $\mathbf{B}^{-1}$, $\mathbf{B}^H$, $\mathbf{B}(p, q)$ and $\mathbf{B}^{(p)}$, respectively. Furthermore, $||\mathbf{B}||_F$ represents the Frobenius norm of $\mathbf{B}$ whereas Tr($\mathbf{B}$) denotes the trace of a matrix $\mathbf{B}$ and $|\mathbf{B}|$ represents its determinant. blkdiag($\mathbf{A}, \mathbf{B}$) is a block diagonal matrix created by diagonal placement of the matrices $\mathbf{A}$ and $\mathbf{B}$; diag($\mathbf{b}$) denotes a diagonal matrix with vector $\mathbf{b}$ on its main diagonal whereas diag($\mathbf{B}$) represents a column vector constructed from the diagonal entries of $\mathbf{B}$. The notation $\mathbb{C}^{R \times T}$ denotes a matrix of size $R \times T$ with complex entries;

an $N \times N$ identity matrix is denoted as $\mathbf{I}_N$ and the expectation operator is represented by $\mathbb{E}[\cdot]$. The complex Gaussian noise distribution with mean $\mathbf{b}$ and covariance matrix $\mathbf{B}$ is denoted as $\mathcal{CN}(\mathbf{b}, \mathbf{B})$.

II. SYSTEM AND CHANNEL MODELS
A. SYSTEM MODEL
Consider the mmWave MSU-MIMO-OFDM downlink underlay CRN depicted in Fig. 1(a), where a CBS with N_t transmit antennas serves M SUs, having N_r receive antennas each, in the presence of a single PU. In addition, as previously mentioned, because the traditional fully-digital architecture necessitates the usage of a separate RF chain for each antenna, we consider a hybrid fully-connected architecture at both the CBS and SUs, similar to [8] and [9] as shown in Fig. 1(b). Furthermore, the CBS and SU transfer information via MN_s length-K data symbol blocks such that $MN_s \leq M_t \leq N_t$ at the CBS and $N_s \leq M_r \leq N_r$ at each SU. The quantities M_t and M_r denote the number of RF chains at the CBS and at each SU, respectively. K signifies the total number of sub-carriers utilized in OFDM signaling, and N_s denotes the number of per-subcarrier data streams for each SU. Note that, for simplicity, we have assumed the number of data streams loaded on each subcarrier to be equal. At the CBS, each symbol vector $\mathbf{s}[k] \in \mathbb{C}^{MN_s \times 1}, k \in \{1, \ldots, K\}$ is initially precoded by the BB-TPC $\mathbf{F}_{BB}[k] \in \mathbb{C}^{M_t \times MN_s}$ and subsequently converted to time domain using M_t IFFT's of length length K. To avoid inter-symbol interference, a cyclic prefix (CP) with duration equal to the maximum delay spread of the channel has been added before applying the RF-TPC $\mathbf{F}_{RF} \in \mathbb{C}^{N_t \times M_t}$. Note that the RF precoding takes place after the IFFT considering the optimal RF-TPC to be frequency flat [9], [20]. Assuming constant AoAs and AoDs for the different multipath components across the subcarriers, the RF-TPCs across subcarriers can be set identically. With this consideration, at subcarrier k, the final discrete-time transmitted signal $\mathbf{x}[k] \in \mathbb{C}^{N_t \times 1}$ can be expressed as

$$\mathbf{x}[k] = \mathbf{F}_{RF}\mathbf{F}_{BB}[k]\mathbf{s}[k], \qquad (1)$$

where $\mathbf{F}_{BB}[k] = [\mathbf{F}_{BB,1}[k], \ldots, \mathbf{F}_{BB,m}[k] \ldots, \mathbf{F}_{BB,M}[k]]$ and $\mathbf{s}[k] = [\mathbf{s}_1^T[k], \ldots, \mathbf{s}_m^T[k], \ldots, \mathbf{s}_M^T[k]]^T$. The term, $\mathbf{s}_m[k]$ denotes the symbol vector for the mth SU on the kth subcarrier that has zero mean and covariance matrix $\mathbf{R}_{ss}[k] = \mathbb{E}[\mathbf{s}[k]\mathbf{s}^H[k]] = \mathbf{I}_{N_s}$. Moreover, $\mathbf{p}[k] = [\mathbf{p}_1^T[k], \ldots, \mathbf{p}_m^T[k], \ldots, \mathbf{p}_M^T[k]]^T \in \mathbb{R}^{MN_s \times 1}$ indicates the optimal power loading vector at subcarrier k, and $p_{m,d}[k]$ corresponds to the optimal power allocated to dth stream of the mth SU on a particular subcarrier k. Since analog phase shifters are used to realize $\mathbf{F}_{RF}$, its elements are constrained to satisfy $|\mathbf{F}_{RF}(i,j)| = \frac{1}{\sqrt{N_t}} \forall i, j$. Further, in the underlay CR system, the interference introduced to the PU by the transmission between the CBS and SUs limits the total transmit power for communication between the CBS and SUs. This paper examines the hybrid RC/TPC design under subcarrier-specific power constraints. One can express the interference experienced by a PU on the subcarrier k, $J_0[k]$,

as

$$J_0[k] = \left\|\mathbf{G}[k]\mathbf{F}_{RF}\mathbf{F}_{BB}[k]\text{diag}(\sqrt{\mathbf{p}[k]})\right\|_F^2, \qquad (2)$$

where $\mathbf{G}[k] \in \mathbb{C}^{N_r \times N_t}$ denotes the equivalent mmWave MIMO-OFDM channel between the CBS and PU. Let I_{th} denote the PU-specified interference threshold per subcarrier. Therefore, the SU is constrained to satisfy $J_0[k] \leq I_{th}$.

Assuming a block-fading channel, the received signal on the kth subcarrier at the mth SU, $m \in \{1, \ldots, M\}$, is given by

$$\begin{aligned}
\mathbf{y}_m[k] &= \mathbf{H}_m[k]\mathbf{x}[k] + \mathbf{n}_m[k], \\
&= \mathbf{H}_m[k]\mathbf{F}_{RF}\mathbf{F}_{BB,m}[k]\mathbf{s}_m[k] \\
&\quad + \sum_{n=1, n\neq m}^{M}\mathbf{H}_m[k]\mathbf{F}_{RF}\mathbf{F}_{BB,n}[k]\mathbf{s}_n[k] + \mathbf{n}_m[k], \qquad (3)
\end{aligned}$$

where $\mathbf{H}_m[k] \in \mathbb{C}^{N_r \times N_t}$ denotes the frequency domain mmWave MIMO channel between the CBS and mth SU, and $\mathbf{n}_m[k] \in \mathbb{C}^{N_r \times 1}$ is the complex Gaussian noise with independent and identically distributed (i.i.d) entries that follow the distribution $\mathcal{CN}(\mathbf{0}, \sigma^2\mathbf{I})$. The signal received at the mth SU is first combined using the RF-RC $\mathbf{W}_{RF,m} \in \mathbb{C}^{N_r \times M_r}$ in the time domain. This is followed by CP removal and conversion back to the frequency domain using M_r FFTs, of size K. Next, the symbols loaded on each subcarrier are combined using the frequency selective BB-RC $\mathbf{W}_{BB,m}[k] \in \mathbb{C}^{M_r \times N_s}$ to obtain the processed received signal $\widetilde{\mathbf{y}}_m[k] \in \mathbb{C}^{N_s \times 1}$ on the kth subcarrier as

$$\begin{aligned}
\widetilde{\mathbf{y}}_m[k] &= \mathbf{W}_{BB,m}^H[k]\mathbf{W}_{RF,m}^H\mathbf{H}_m[k]\mathbf{F}_{RF}\mathbf{F}_{BB,m}[k]\mathbf{s}_m[k] \\
&\quad + \sum_{n=1, n\neq m}^{M}\mathbf{W}_{BB,m}^H[k]\mathbf{W}_{RF,m}^H\mathbf{H}_m[k]\mathbf{F}_{RF}\mathbf{F}_{BB,n}[k]\mathbf{s}_n[k] \\
&\quad + \mathbf{W}_{BB,m}^H[k]\mathbf{W}_{RF,m}^H\mathbf{n}_m[k], \qquad (4)
\end{aligned}$$

Note that, similar to the RF-TPC $\mathbf{F}_{RF}$, the elements of the RF-RC at each SU are constrained to satisfy $|\mathbf{W}_{RF,m}(i,j)| = \frac{1}{\sqrt{N_r}}, \forall i, j$.

B. CHANNEL MODEL
In a practical wideband mmWave MIMO propagation environment, tightly packed antenna array transceivers and limited scatterers lead to strong spatial correlation. Therefore, it is critical to model realistic correlated channels to accurately predict the performance of wideband mmWave MIMO systems. Hence, we adopt the geometric mmWave clustered parametric channel model based on the extended Saleh-Valenzuela model to accurately capture the spatial properties of practical mmWave MIMO-OFDM CRNs [6], [32]. This has been validated by measurements [33], [34], and variations of this model have been approved by the 3GPP Technical Specification Group [35] as part of their standardization efforts. As per this model, the dth delay tap of the downlink mmWave MIMO-OFDM channel matrix between the CBS and mth SU, denoted by $\mathbf{H}_m[d]$, is generated as the sum of the contributions of N_{cl} scattering clusters, each
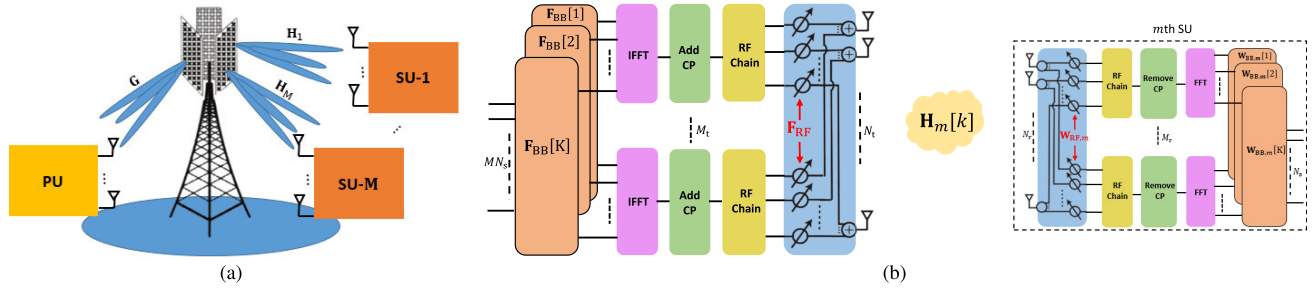
FIGURE 1. (a) MIMO-OFDM downlink underlay CRN (b) Hybrid transceiver design adopted at the CBS and the *m*th SU.

of which comprises of N_p propagation paths. Each cluster c is assumed to have a time delay $\tau_{c,m}$ whereas, each path $l = 1, 2, \ldots, N_p$, within a cluster, has a relative time delay of $\tau_{l,m}$. Therefore, the matrix $\mathbf{H}_m[d]$ corresponding to the dth delay tap of the mmWave MIMO-OFDM channel can be written as

$$
\begin{aligned}
&\mathbf{H}_m(d) \\
&= \gamma \sum_{c=1}^{N_{cl}} \sum_{l=1}^{N_p} \alpha_{cl,m} p_{\mathrm{rc}}(dT_{\mathrm{s}} - \tau_{c,m} - \tau_{l,m}) \beta_{\mathrm{r}}(\phi_{cl,m}^{\mathrm{r}}, \theta_{cl,m}^{\mathrm{r}}) \\
&\quad \times \beta_{\mathrm{t}}(\phi_{cl,m}^{\mathrm{t}}, \theta_{cl,m}^{\mathrm{t}}) \mathbf{a}_{\mathrm{r}}(\phi_{cl,m}^{\mathrm{r}}, \theta_{cl,m}^{\mathrm{r}}) \mathbf{a}_{\mathrm{t}}^H(\phi_{cl,m}^{\mathrm{t}}, \theta_{cl,m}^{\mathrm{t}}),
\end{aligned}
\tag{5}
$$

where $\gamma = \sqrt{\frac{N_r N_t}{N_{cl} N_p}}$ is a normalization parameter and $\alpha_{cl,m}$ is the complex gain of the lth path in the cth scattering cluster. Furthermore, $(\phi_{cl,m}^{\mathrm{r}}, \theta_{cl,m}^{\mathrm{r}})$ and $(\phi_{cl,m}^{\mathrm{t}}, \theta_{cl,m}^{\mathrm{t}})$ are the azimuth, elevation pairs for the angle of arrival (AoA) and departure (AoD), respectively, of the lth path in the cth scattering cluster. The quantities $\beta_{\mathrm{r}}(\phi_{cl,m}^{\mathrm{r}}, \theta_{cl,m}^{\mathrm{r}})$ and $\beta_{\mathrm{t}}(\phi_{cl,m}^{\mathrm{t}}, \theta_{cl,m}^{\mathrm{t}})$ denote the receive and transmit antenna gains at the corresponding AoA and AoD. Further, $p_{\mathrm{rc}}(dT_s - \tau_{c,m} - \tau_{l,m})$ denotes the T_s-spaced pulse-shaping function at time-delay $(\tau_{c,m} + \tau_{l,m})$. Finally, $\mathbf{a}_{\mathrm{r}}(\phi_{cl,m}^{\mathrm{r}}, \theta_{cl,m}^{\mathrm{r}})$ and $\mathbf{a}_{\mathrm{t}}(\phi_{cl,m}^{\mathrm{t}}, \theta_{cl,m}^{\mathrm{t}})$ represent the normalized array response vectors at the receiver and transmitter, respectively, for the AoA pair $(\phi_{cl,m}^{\mathrm{r}}, \theta_{cl,m}^{\mathrm{r}})$ and AoD pair $(\phi_{cl,m}^{\mathrm{t}}, \theta_{cl,m}^{\mathrm{t}})$. Moreover, note that, the model for $\mathbf{a}_{\mathrm{r}}(\phi_{cl,m}^{\mathrm{r}}, \theta_{cl,m}^{\mathrm{r}})$ and $\mathbf{a}_{\mathrm{t}}(\phi_{cl,m}^{\mathrm{t}}, \theta_{cl,m}^{\mathrm{t}})$ are dependent on the type of the antenna array structures used at the receiver and transmitter, respectively. In this paper, we consider URPAs at both the receiver and transmitter ends since they allow for the packaging of a large number of antenna elements in a relatively small area, thus enabling 3D beamforming that can lead to remarkably enhanced array gain and directivity. This has been shown to be significantly appealing for mmWave transceiver design [36]. Consider a URPA in the YZ plane, with N_{y} antenna elements with inter-antenna spacing d_{y} and N_{z} antenna elements with antenna spacing d_{z}, on the Y and Z axes, respectively. The expression for the array response vector corresponding to azimuth angle ϕ_{cl} and an elevation angle θ_{cl} is given as [37]

$$
\begin{aligned}
&\mathbf{a}_{\mathrm{URPA}}(\phi_{cl}, \theta_{cl}) \\
&= \frac{1}{\sqrt{N}}[1, \ldots, e^{jkd(p\sin(\phi_{cl})\sin(\theta_{cl}) + q\cos(\theta_{cl}))}, \\
&\qquad \ldots, e^{jkd((N_{\mathrm{y}}-1)\sin(\phi_{cl})\sin(\theta_{cl}) + (N_{\mathrm{z}}-1)\cos(\theta_{cl}))}]^T,
\end{aligned}
\tag{6}
$$

where $k = \frac{2\pi}{\lambda}$ is the wave number, $d_{\mathrm{y}} = d_{\mathrm{z}} = d$, p, q denote the antenna indices such that $0 \leq p \leq N_{\mathrm{y}} - 1$ and $0 \leq q \leq N_{\mathrm{z}} - 1$, and $N = N_{\mathrm{y}} N_{\mathrm{z}}$. Using the time-domain model for $\mathbf{H}_m(d)$ in (5), the frequency-domain MIMO channel at the kth subcarrier, denoted by $\mathbf{H}_m[k]$, can be expressed as [8]

$$
\mathbf{H}_m[k] = \sum_{d=0}^{N_{tap}-1} \mathbf{H}_m(d) e^{-j\frac{2\pi k}{K} d}.
\tag{7}
$$

Using the fact that the array response vectors are independent of the subcarriers, Eq. (7) can also be written in the compact form

$$
\mathbf{H}_m[k] = \mathbf{A}_{\mathrm{r},m} \mathrm{diag}(\widetilde{\boldsymbol{\alpha}}_m[k]) \mathbf{A}_{\mathrm{t},m}^H,
\tag{8}
$$

where, $\mathbf{A}_{\mathrm{r},m} \in \mathbb{C}^{N_r \times N_{cl} N_p}$, $\mathbf{A}_{\mathrm{t},m} \in \mathbb{C}^{N_t \times N_{cl} N_p}$, and $\tilde{\boldsymbol{\alpha}}_m[k] \in \mathbb{C}^{N_{cl} N_p \times 1}$ are given by

$$
\begin{aligned}
\mathbf{A}_{\mathrm{r},m} &= [\mathbf{a}_{\mathrm{r}}(\phi_{11,m}^{\mathrm{r}}, \theta_{11,m}^{\mathrm{r}}), \ldots, \mathbf{a}_{\mathrm{r}}(\phi_{N_{cl}N_p,m}^{\mathrm{r}}, \theta_{N_{cl}N_p,m}^{\mathrm{r}})] \\
\mathbf{A}_{\mathrm{t},m} &= [\mathbf{a}_{\mathrm{t}}(\phi_{11,m}^{\mathrm{t}}, \theta_{11,m}^{\mathrm{t}}), \ldots, \mathbf{a}_{\mathrm{t}}(\phi_{N_{cl}N_p,m}^{\mathrm{t}}, \theta_{N_{cl}N_p,m}^{\mathrm{t}})], \\
\tilde{\boldsymbol{\alpha}}_m[k] &= [\bar{\alpha}_{11,m}[k], \ldots, \bar{\alpha}_{cl,m}[k], \ldots \bar{\alpha}_{N_{cl}N_p,m}[k]], \text{ and} \\
\bar{\alpha}_{cl,m}[k] &= \sum_{d=0}^{N_{tap}-1} \alpha_{cl,m} p_{\mathrm{rc}}(dT_{\mathrm{s}} - \tau_{c,m} - \tau_{l,m}) e^{-j\frac{2\pi k}{K} d}.
\end{aligned}
\tag{9}
$$

The problem formulation corresponding to hybrid transceiver design is presented in the next subsection.

C. HYBRID TRANSCEIVER DESIGN PROBLEM

This section presents the framework for design of the hybrid RCs $\{\mathbf{W}_{\mathrm{RF},m}, \mathbf{W}_{\mathrm{BB},m}[k]\}_{m,k=1}^{M,K}$, hybrid TPCs $\mathbf{F}_{\mathrm{RF}}, \{\mathbf{F}_{\mathrm{BB}}[k]\}_{k=1}^{K}$, and the optimal power loading vector $\{\mathbf{p}[k]\}_{k=1}^{K}$, such that the overall SE of SU-transmission is maximized. Furthermore, the interference experienced by the PU per each subcarrier is required to not exceed the threshold I_{th}, while the subcarrier power at the CBS is restricted to $P_{\max}$. The SE of the system can be written as

$$
\mathcal{R}_{\mathrm{sum}} = \frac{1}{K} \sum_{m=1}^{M} \sum_{k=1}^{K} \mathcal{R}_m[k],
\tag{10}
$$

where $\mathcal{R}_m[k]$ is the SE of the mth SU at the subcarrier k. For Gaussian signalling, $\mathcal{R}_m[k]$ can be expressed as

$$
\mathcal{R}_m[k] = \log_2\left(\left|I_{N_s} + \mathbf{R}_{\mathrm{in},m}^{-1}[k] \Gamma_m[k]\right|\right),
\tag{11}
$$

where $\Gamma_m[k]$ and $\mathbf{R}_{\text{in},m}^{-1}[k]$ denote the desired signal covariance and the interference-plus-noise covariance matrices of $\widetilde{\mathbf{y}}_m[k]$, respectively, and can be derived as shown in (12) and (13), at the bottom of the page. Therefore, one can formulate the SE maximization problem as

$$\max_{\left\{\mathbf{W}_{\text{RF},m},\mathbf{W}_{\text{BB},m}[k],\mathbf{F}_{\text{RF}},\mathbf{F}_{\text{BB}}[k],\mathbf{p}[k]\right\}_{m,k=1}^{M,K}} \mathcal{R}_{\text{sum}}$$

$$\text{s.t.} \begin{cases} |\mathbf{F}_{\text{RF}}(i,j)| = \dfrac{1}{\sqrt{N_{\text{t}}}}, \forall i,j, \\ |\mathbf{W}_{\text{RF},m}(i,j)| = \dfrac{1}{\sqrt{N_{\text{r}}}}, \forall i,j,m, \\ J_0[k] \leq I_{\text{th}}, \forall k, \\ \left\|\mathbf{F}_{\text{RF}}\mathbf{F}_{\text{BB}}[k]\text{diag}(\sqrt{\mathbf{p}[k]})\right\|_F^2 \leq P_{\max}, \forall k. \end{cases} \tag{14}$$

One can readily observe that maximizing (14) directly requires an apparent five-matrix-variable joint optimization over $\left(\left\{\mathbf{W}_{\text{RF},m},\mathbf{W}_{\text{BB},m}[k],\mathbf{F}_{\text{RF}},\mathbf{F}_{\text{BB}}[k],\mathbf{p}[k]\right\}_{m,k=1}^{M,K}\right)$. However, solving the joint optimization problem is infeasible because the objective function and constant magnitude constraints on the elements of the RF-RC $\mathbf{W}_{\text{RF},m}$ and RF-TPC $\mathbf{F}_{\text{RF}}$ are non-convex in nature. The problem (14) is thus decoupled as follows: First, each SU constructs its own blind hybrid MMSE-RC $\left\{\mathbf{W}_{\text{RF},m},\mathbf{W}_{\text{BB},m}[k]\right\}_{m,k=1}^{M,K}$, assuming the optimal per-subcarrier FD-TPC with blind equal power loading for each stream at CBS. The second phase involves designing the hybrid TPC $\mathbf{F}_{\text{RF}},\left\{\mathbf{F}_{\text{BB}}\right\}_{k=1}^{K}$, at CBS based on the knowledge of effective channel at each SU and each subcarrier, given by $\left\{\mathbf{W}_{\text{RF},m},\mathbf{W}_{\text{BB},m}[k],\mathbf{H}_m[k]\right\}_{m,k=1}^{M,K}$. This is followed by the determination of the optimal power loading vector $\left\{\mathbf{p}[k]\right\}_{k=1}^{K}$. The following sections present an in depth description of the algorithms for each of these steps.

III. BLIND HYBRID MMSE-RC DESIGN
In the downlink CRN, each SU designs the appropriate hybrid RC based on the estimated downlink channel $\left\{\mathbf{H}_m[k]\right\}_{k=1}^{K}$ and then reports the effective CSI, $\left\{\mathbf{H}_m^{\text{eff}}[k]\right\}_{k=1}^{K}$ back to CBS for downlink communication. Toward this end, each SU initially designs the optimal FD-TPC $\bar{\mathbf{F}}_m^{\text{opt}}[k] = [\bar{\mathbf{F}}_1[k],\ldots,\bar{\mathbf{F}}_m[k],\ldots,\bar{\mathbf{F}}_M[k]] \in \mathbb{C}^{N_{\text{t}} \times MN_{\text{s}}}, \forall k$ to suppress both the MUI and ISI. For this purpose, consider the SVD of the mmWave MIMO channel at kth subcarrier, $\mathbf{H}_m[k]$ given

as

$$\mathbf{H}_m[k]$$
$$= \mathbf{U}_m[k]\Sigma_m[k]\mathbf{V}_m^H[k]$$
$$= \begin{bmatrix} \mathbf{U}_m^1[k] & \mathbf{U}_m^2[k] \end{bmatrix} \begin{bmatrix} \Sigma_m^1[k] & 0 \\ 0 & \Sigma_m^2[k] \end{bmatrix} \begin{bmatrix} \mathbf{V}_m^1[k] & \mathbf{V}_m^2[k] \end{bmatrix}^H, \tag{15}$$

where $\mathbf{U}_m^1[k]$ and $\mathbf{V}_m^1[k]$ consist of the initial N_{s} columns of $\mathbf{U}_m[k]$ and $\mathbf{V}_m[k]$, respectively. To achieve the required $\left\{\bar{\mathbf{F}}_m^{\text{opt}}[k]\right\}_{k=1}^{K}$, we set $\bar{\mathbf{F}}_m[k] = \mathbf{V}_m^1[k]$ and $\bar{\mathbf{F}}_{i,i\neq m}[k] = \widetilde{\mathbf{V}}_m^2[k]$, where $\widetilde{\mathbf{V}}_m^2[k]$ consists of the last N_{s} columns of $\mathbf{V}_m^2[k]$, i.e., $\widetilde{\mathbf{V}}_m^2[k] \in \mathcal{N}(\mathbf{H}_m[k])$. Furthermore, since the SU does not have knowledge of the downlink channel matrices $\left\{\mathbf{G}[k]\right\}_{k=1}^{K}$ between the CBS and PU, a blind equal power allocation is considered for all the streams while designing the hybrid MMSE-RC at each SU. Assuming $\bar{\mathbf{F}}_m^{\text{opt}}[k]$ at the CBS, the signal received at the mth SU on the kth subcarrier, $\bar{\mathbf{y}}_m[k] \in \mathbb{C}^{N_{\text{r}} \times 1}$, can be expressed as

$$\bar{\mathbf{y}}_m[k] = \sqrt{\rho_m[k]}\mathbf{H}_m[k]\bar{\mathbf{F}}_m^{\text{opt}}[k]\mathbf{s}[k] + \mathbf{n}_m[k], \tag{16}$$

where $\rho_m[k] = \dfrac{I_{\text{th}}}{\left\|\mathbf{G}[k]\bar{\mathbf{F}}_m^{\text{opt}}[k])\right\|_F^2}$, which is derived by equally dividing the interference threshold I_{th} among the MN_{s} data streams. Upon employing $\bar{\mathbf{F}}_m^{\text{opt}}[k]$, Eq. (16) can be rewritten as

$$\bar{\mathbf{y}}_m[k] = \sqrt{\rho_m[k]}\mathbf{U}_m^1[k]\Sigma_m^1[k]\mathbf{s}_m[k] + \mathbf{n}_m[k]. \tag{17}$$

Therefore, the design problem for hybrid MMSE-RC at the mth SU can be stated as follows

$$\left(\mathbf{W}_{\text{RF},m}^{\text{opt}},\left\{\mathbf{W}_{\text{BB},m}^{\text{opt}}[k]\right\}_{k=1}^{K}\right) =$$

$$\arg\min_{\mathbf{W}_{\text{RF},m},\left\{\mathbf{W}_{\text{BB},m}[k]\right\}_{k=1}^{K}} \frac{1}{K}\sum_{k=1}^{K}\mathbb{E}\Big\{\Big\|\mathbf{s}_m[k]$$

$$- \mathbf{W}_{\text{BB},m}^H[k]\mathbf{W}_{\text{RF},m}^H\bar{\mathbf{y}}_m[k]\Big\|_2^2\Big\},$$

$$\text{s.t. } \left|\mathbf{W}_{\text{RF},m}(i,j)\right| = \frac{1}{\sqrt{N_{\text{r}}}}.\forall i,j. \tag{18}$$

It is clear from Eq.(18) that the objective above is to reduce the MSE (mean squared error) between the combined received signal $\mathbf{W}_{\text{BB},m}^H[k]\mathbf{W}_{\text{RF},m}^H\bar{\mathbf{y}}_m[k]$ and the transmitted symbol vector $\mathbf{s}_m[k]$. Observe that, without the elements'

$$\Gamma_m[k] = \mathbf{W}_{\text{BB},m}^H[k]\mathbf{W}_{\text{RF},m}^H\mathbf{H}_m[k]\mathbf{F}_{\text{RF}}\mathbf{F}_{\text{BB},m}[k]\text{diag}(\mathbf{p}_m[k])\mathbf{F}_{\text{BB},m}^H[k]\mathbf{F}_{\text{RF}}^H\mathbf{H}_m^H[k]\mathbf{W}_{\text{RF},m}\mathbf{W}_{\text{BB},m}[k]\Big), \tag{12}$$

$$\mathbf{R}_{\text{in},m}[k] = \underbrace{\sum_{n=1,n\neq m}^{M}\Big(\mathbf{W}_{\text{BB},m}^H[k]\mathbf{W}_{\text{RF},m}^H\mathbf{H}_m[k]\mathbf{F}_{\text{RF}}\mathbf{F}_{\text{BB},n}[k]\text{diag}(\mathbf{p}_n[k])\mathbf{F}_{\text{BB},n}^H[k]\mathbf{F}_{\text{RF}}^H\mathbf{H}_m^H[k]\mathbf{W}_{\text{RF},m}\mathbf{W}_{\text{BB},m}[k]\Big)}_{\text{interference covariance},\mathbf{R}_{\text{i},m}[k]}$$

$$+ \underbrace{\sigma^2\mathbf{W}_{\text{BB},m}^H[k]\mathbf{W}_{\text{RF},m}^H\mathbf{W}_{\text{RF},m}\mathbf{W}_{\text{BB},m}[k]}_{\text{noise covariance},\mathbf{R}_{\text{n},m}[k]}. \tag{13}$$

constant-magnitude restrictions in $\mathbf{W}_{\mathrm{RF},m}$, the solution to (18) is equivalent to the linear MMSE RC $\mathbf{W}_{\mathrm{MMSE},m}^{H}[k] \in \mathbb{C}^{N_s \times N_r}$ that is given as [38]

$$\mathbf{W}_{\mathrm{MMSE},m}^{H}[k] = \mathbf{R}_{s\bar{y},m}[k] \mathbf{R}_{\bar{y}\bar{y},m}^{-1}[k]. \qquad (19)$$

Following a procedure similar to our earlier work [30] for a particular subcarrier k, one can obtain the expression for $\mathbf{W}_{\mathrm{MMSE},m}^{H}[k]$ as

$$\mathbf{W}_{\mathrm{MMSE},m}^{H}[k]$$
$$= \frac{1}{\sqrt{\rho_m[k]}} \Sigma_m^1[k] \left((\Sigma_m^1[k])^2 + \frac{\sigma^2}{\rho_m[k]} \mathbf{I}_{N_s} \right)^{-1} (\mathbf{U}_m^1[k])^H. \qquad (20)$$

Note that calculation of $\mathbf{W}_{\mathrm{MMSE},m}^{H}[k]$ involves the inversion of a diagonal matrix $\left((\Sigma_m^1[k])^2 + \frac{\sigma^2}{\rho_m[k]} \mathbf{I}_{N_s} \right)$, due to which the computational complexity of the scheme is low. Furthermore, as derived in [6], the optimization problem in (18) can be further reduced to

$$\left(\mathbf{W}_{\mathrm{RF},m}^{\mathrm{opt}}, \{ \mathbf{W}_{\mathrm{BB},m}^{\mathrm{opt}}[k] \}_{k=0}^{K-1} \right) =$$
$$\arg \min_{\mathbf{W}_{\mathrm{RF},m}, \{ \mathbf{W}_{\mathrm{BB},m}[k] \}_{k=0}^{K-1}} \sum_{k=0}^{K-1} \left\| \mathbf{R}_{\bar{y}\bar{y},m}^{\frac{1}{2}}[k] \left(\mathbf{W}_{\mathrm{MMSE},m}[k] \right. \right.$$
$$\left. \left. - \mathbf{W}_{\mathrm{RF},m} \mathbf{W}_{\mathrm{BB},m}[k] \right) \right\|_F^2,$$
$$\mathrm{s.}t. \quad \left| \mathbf{W}_{\mathrm{RF},m}(i,j) \right| = \frac{1}{\sqrt{N_r}}, \forall i, j. \qquad (21)$$

Note that in (21), the RF combiner $\mathbf{W}_{\mathrm{RF},m}$ needs to be jointly optimized across all the subcarriers, whereas the BB combiner $\mathbf{W}_{\mathrm{BB},m}[k]$ can be locally optimized for each individual subcarrier, which renders the SOMP approach developed in Algorithm 2 of [6] inapplicable for this problem. In this paper, we propose a modified SOMP (MSOMP) technique that can be readily applied to tackle the optimization problem above. In addition, the authors in [6] assume availability of the true AoAs to construct the matrix $\mathbf{A}_{\mathrm{r},m}$, which is infeasible in practice. Thus, for practical implementation, we propose to consider only a codebook rather than the matrix $\mathbf{A}_{\mathrm{r},m}$ that contains the array response vectors for the true AoAs. To create the codebook, the azimuth angular range $[\phi_{\min}, \phi_{\max}]$ and elevation angular range $[\theta_{\min}, \theta_{\max}]$ are quantized using N_ϕ and N_θ bits, respectively, and form the matrix of jointly quantized response vectors of size $N_r \times 2^{N_\phi + N_\theta}$ as

$$\mathbf{A}_{\mathrm{r}}^{\mathrm{q}} = \left[\mathbf{a}_{\mathrm{r}}(\phi_1^{\mathrm{r}}, \theta_1^{\mathrm{r}}), \ldots, \mathbf{a}_{\mathrm{r}}(\phi_i^{\mathrm{r}}, \theta_l^{\mathrm{r}}), \ldots, \mathbf{a}_{\mathrm{r}}(\phi_{2^{N_\phi}}^{\mathrm{r}}, \theta_{2^{N_\theta}}^{\mathrm{r}}) \right]. \qquad (22)$$

To jointly design $\mathbf{W}_{\mathrm{RF},m}$ across all the subcarriers, the MSOMP approach begins by initializing the matrix $\mathbf{W}_{\mathrm{MMSE},m} \in \mathbb{C}^{KN_r \times KN_s}$, which is a block diagonal matrix comprising of the optimal fully digital MMSE combiners $\mathbf{W}_{\mathrm{MMSE},m}[k], \forall k$ along its main diagonal as $\mathbf{W}_{\mathrm{MMSE},m} = \mathrm{blkdiag}(\mathbf{W}_{\mathrm{MMSE},m}[1], \ldots, \mathbf{W}_{\mathrm{MMSE},m}[K])$. Similarly, the

matrix $\mathbf{R}_{\bar{y}\bar{y},m} \in \mathbb{C}^{N_r \times KN_r}$ is constructed by concatenating the output signal covariance matrices $\mathbf{R}_{\bar{y}\bar{y},m}[k]$ for the different subcarriers as $\mathbf{R}_{\bar{y}\bar{y},m} = [\mathbf{R}_{\bar{y}\bar{y},m}[1], \ldots, \mathbf{R}_{\bar{y}\bar{y},m}[K]]$. As a result, in each iteration, it is possible to determine the column index n of the quantized response vectors $\mathbf{A}_{\mathrm{r}}^{\mathrm{q}}$ along which the previous residue $\mathbf{W}_{\mathrm{res},m}$ has the maximum weighted projection jointly across all the subcarriers. Once we obtain the solution for $\mathbf{W}_{\mathrm{RF},m}$, the per subcarrier optimization problem given below is solved to update $\mathbf{W}_{\mathrm{BB},m}[k]$.

$$\{ \overline{\mathbf{W}}_{\mathrm{BB},m}^{\mathrm{opt}}[k] \}_{k=1}^{K} =$$
$$\arg \min_{\{ \mathbf{W}_{\mathrm{BB},m}[k] \}_{k=1}^{K}} \left\| \mathbf{R}_{\bar{y}\bar{y},m}^{\frac{1}{2}}[k] (\mathbf{W}_{\mathrm{MMSE},m}[k] - \mathbf{A}_{\mathrm{r}}^{\mathrm{q}} \overline{\mathbf{W}}_{\mathrm{BB},m}[k]) \right\|_F^2,$$
$$\mathrm{s.}t. \quad \left\| \mathrm{diag}(\overline{\mathbf{W}}_{\mathrm{BB},m}[k] \overline{\mathbf{W}}_{\mathrm{BB},m}^{H}[k]) \right\|_0 = M_{\mathrm{r}}, \forall k. \qquad (23)$$

Note that, the quantities $\mathbf{A}_{\mathrm{r}}^{\mathrm{q}}$ and $\{ \overline{\mathbf{W}}_{\mathrm{BB},m}[k] \}_{k=1}^{K}$ in (23) act as auxiliary variables from which one obtains $\mathbf{W}_{\mathrm{RF},m}^{\mathrm{opt}}$ and $\{ \mathbf{W}_{\mathrm{BB},m}^{\mathrm{opt}}[k] \}_{k=0}^{K-1}$, respectively. The sparsity constraint $\left\| \mathrm{diag}(\overline{\mathbf{W}}_{\mathrm{BB},m}[k] \overline{\mathbf{W}}_{\mathrm{BB},m}^{H}[k]) \right\|_0 = M_{\mathrm{r}}, \forall k$ in (23) implies that the number of non zero rows of $\overline{\mathbf{W}}_{\mathrm{BB},m}[k] \forall k$ cannot be greater than M_{r}. The summary of the overall proposed MSOMP based blind combiner design at each SU is given in Algorithm 1. The key steps of this algorithm are now discussed below.

In each iteration, steps 4 and 5 determine the column index n of the quantized response vectors $\mathbf{A}_{\mathrm{r}}^{\mathrm{q}}$ along which the previous residue $\mathbf{W}_{\mathrm{res},m}$ yields the highest weighted projection across all the subcarriers. The matrix $\mathbf{W}_{\mathrm{RF},m}$ is updated in step 6 by concatenating the nth column of $\mathbf{A}_{\mathrm{r}}^{\mathrm{q}}$. Step 7 initializes both $\mathbf{W}_{\mathrm{res},m}, \mathbf{W}_{\mathrm{BB},m}$ to compute the BB combiner locally. Step 9 next computes the BB combiner $\mathbf{W}_{\mathrm{BB},m}[k]$ using the weighted least squares solution over $\mathbf{R}_{\bar{y}\bar{y},m}[k]$ for the kth subcarrier. Step 10 calculates the corresponding residue matrix $\mathbf{W}_{\mathrm{res},m}[k]$ for each subcarrier and subsequently builds a new block-diagonal residue matrix $\mathbf{W}_{\mathrm{res},m}$ in step 11 which is utilized in the following iteration. After M_{r} columns have been added to $\mathbf{W}_{\mathrm{RF},m}$, the algorithm concludes and returns the hybrid RC $\mathbf{W}_{\mathrm{RF},m}$ and $\{ \mathbf{W}_{\mathrm{BB},m}[k] \}_{k=1}^{K}$. Lastly, the SU feeds back its effective CSI, $\{ \mathbf{H}_m^{\mathrm{eff}}[k] = \mathbf{W}_{\mathrm{BB},m}^{H}[k] \mathbf{W}_{\mathrm{RF},m}^{H} \mathbf{H}_m[k] \}_{k=1}^{K}$ to the CBS for use in the creation of the hybrid TPCs and the allocation of optimal power, as explained in detail in the following sections.

IV. HYBRID TPC DESIGN AND OPTIMAL POWER LOADING

Using the knowledge of effective channel $\mathbf{H}_m^{\mathrm{eff}}[k] \forall m, k$, obtained via feedback, this section develops the hybrid TPC $\mathbf{F}_{\mathrm{RF}}, \{ \mathbf{F}_{\mathrm{BB}}[k] \}_{k=1}^{K}$ followed by deriving the optimal power loading vector $\{ \mathbf{p}[k] \}_{k=1}^{K}$ at the CBS, aiming to maximize the SE. Therefore, the associated design problem at the CBS can

be expressed as

$$\max_{\{\mathbf{F}_{\mathrm{RF}},\mathbf{F}_{\mathrm{BB}}[k],\mathbf{p}[k]\}_{k=1}^{K}} \frac{1}{K}\sum_{m=1}^{M}\sum_{k=1}^{K}\mathcal{R}_m[k]$$

$$\text{s.t.}\begin{cases} |\mathbf{F}_{\mathrm{RF}}(i,j)| = \dfrac{1}{\sqrt{N_{\mathrm{t}}}}, \forall i,j, \\ J_0[k] \le I_{\mathrm{th}}, \forall k, \\ \left\|\mathbf{F}_{\mathrm{RF}}\mathbf{F}_{\mathrm{BB}}[k]\mathrm{diag}(\sqrt{\mathbf{p}[k]})\right\|_F^2 \le P_{\max}, \forall k \end{cases} \quad (24)$$

where $\mathcal{R}_m[k]$ is given by (11). Consider the SVD of $\mathbf{H}_m^{\mathrm{eff}}[k]$ as

$$\mathbf{H}_m^{\mathrm{eff}}[k] = \mathbf{U}_m^{\mathrm{eff}}[k]\mathbf{\Sigma}_m^{\mathrm{eff}}[k](\mathbf{V}_m^{\mathrm{eff}}[k])^H$$
$$= \mathbf{U}_m^{\mathrm{eff}}[k]\left[\mathbf{\Sigma}_m^{\mathrm{eff},1}[k]\mathbf{0}\right]\left[\mathbf{V}_m^{\mathrm{eff},1}[k]\mathbf{V}_m^{\mathrm{eff},2}[k]\right]^H, \quad (25)$$

where $\mathbf{\Sigma}_m^{\mathrm{eff},1}[k] \in \mathbb{C}^{N_{\mathrm{s}}\times N_{\mathrm{s}}}$ and $\mathbf{V}_m^{\mathrm{eff},1}[k] \in \mathbb{C}^{N_{\mathrm{t}}\times N_{\mathrm{s}}}$ denote the initial N_{s} columns of the matrices $\mathbf{\Sigma}_m^{\mathrm{eff}}[k]$ and $\mathbf{V}_m^{\mathrm{eff}}[k]$, respectively. Recall that $\mathbf{F}_{\mathrm{RF}}$ is common for all the SUs and all subcarriers, whereas the BB-TPC, which is defined as $\mathbf{F}_{\mathrm{BB}}[k] = [\mathbf{F}_{\mathrm{BB},1}[k],\ldots,\mathbf{F}_{\mathrm{BB},m}[k],\ldots,\mathbf{F}_{\mathrm{BB},M}[k]]$, where $\mathbf{F}_{\mathrm{BB},m}[k]$ denotes the BB-TPC of the mth SU at the kth subcarrier, is unique for each SU and subcarrier. Furthermore, note that the design of $\mathbf{F}_{\mathrm{BB}}[k]$ should target mitigation of the MUI among the SUs. Toward this, we split each SU's BB-TPC into two sub-matrices such that $\mathbf{F}_{\mathrm{BB},m}[k] = \mathbf{F}_{\mathrm{BB},m}^1[k]\mathbf{F}_{\mathrm{BB},m}^2[k]$. Considering, the SVD of $\mathbf{H}_m^{\mathrm{eff}}[k]$ as mentioned in Eq. (25), the decomposition of the BB-TPC as $\mathbf{F}_{\mathrm{BB},m}[k] = \mathbf{F}_{\mathrm{BB},m}^1[k]\mathbf{F}_{\mathrm{BB},m}^2[k]$, and by employing a procedure similar to [30], $\mathcal{R}_m[k]$ can be closely approximated as

$$\mathcal{R}_m[k] \approx \log_2\left(\left|I_{N_{\mathrm{s}}} + (\mathbf{F}_{\mathrm{BB},m}^2[k])^H(\mathbf{\Sigma}_m^{\mathrm{eff},1}[k])^H(\mathbf{U}_m^{\mathrm{eff}}[k])^H\right.\right.$$
$$\left.\times \mathbf{R}_{in,m}^{-1}[k]\mathbf{U}_m^{\mathrm{eff}}[k]\mathbf{\Sigma}_m^{\mathrm{eff},1}[k]\mathbf{F}_{\mathrm{BB},m}^2[k]\mathrm{diag}(\mathbf{p}_m[k])\right|\right)$$
$$-\left(N_{\mathrm{s}} - \left\|(\mathbf{V}_m^{\mathrm{eff},1}[k])^H\mathbf{F}_{\mathrm{RF}}\mathbf{F}_{\mathrm{BB},m}^1[k]\right\|_F^2\right). \quad (26)$$

Observe that in (26), the dependency of $\mathcal{R}_m[k]$ on $\mathbf{F}_{\mathrm{RF}}$ and $\mathbf{F}_{\mathrm{BB},m}^1[k]$ is through the second term, whereas $\mathbf{F}_{\mathrm{BB},m}^2[k]$ and $\mathrm{diag}(\mathbf{p}_m[k])$ impact the first term. Thus, the TPC design procedure at the CBS can be divided into two stages. In the first stage, the RF-TPC $\mathbf{F}_{\mathrm{RF}}$ and BB-TPC $\mathbf{F}_{\mathrm{BB}}^1[k] = [\mathbf{F}_{\mathrm{BB},1}^1[k],\ldots,\mathbf{F}_{\mathrm{BB},m}^1[k],\ldots,\mathbf{F}_{\mathrm{BB},M}^1[k]] \in \mathbb{C}^{M_{\mathrm{t}}\times MN_{\mathrm{s}}}$ can be jointly designed using the capacity-optimal FD-TPC approximation problem, whereas the BB-TPC $\mathbf{F}_{\mathrm{BB}}^2[k] = [\mathbf{F}_{\mathrm{BB},1}^2[k],\ldots,\mathbf{F}_{\mathrm{BB},m}^2[k],\ldots,\mathbf{F}_{\mathrm{BB},M}^2[k]] \in \mathbb{C}^{N_{\mathrm{s}}\times MN_{\mathrm{s}}}$ can be constructed in the second stage with the goal of mitigating the MUI. It is important to emphasize that we impose a unitary power constraint during the design of the stage-1 hybrid TPCs such that $\mathbf{F}_{\mathrm{RF}}\mathbf{F}_{\mathrm{BB}}^1[k] \in \mathcal{U}_{N_{\mathrm{t}}\times MN_{\mathrm{s}}} \forall k = 1,2,\ldots,K$, where $\mathcal{U}_{N_{\mathrm{t}}\times MN_{\mathrm{s}}}$ denotes the set of semi-unitary matrices $\mathcal{U}_{N_{\mathrm{t}}\times MN_{\mathrm{s}}} = \{\mathbf{U} \in \mathbb{C}^{N_{\mathrm{t}}\times MN_{\mathrm{s}}}|\mathbf{U}^H\mathbf{U} = \mathbf{I}\}$. Following the design of hybrid TPC, the interference and transmit power budget constraints are satisfied with the optimal power loading solution.

Algorithm 1 Hybrid-MMSE Combiner Design via MSOMP at the mth SU

Require: $\mathbf{W}_{\mathrm{MMSE},m}, \mathbf{R}_{\bar{y}\bar{y},m}$
1: $\mathbf{W}_{\mathrm{RF},m} = [\,]$ (i.e., Empty Matrix)
2: $\mathbf{W}_{\mathrm{res},m} = \mathbf{W}_{\mathrm{MMSE},m}$
3: **for** $i \le M_{\mathrm{r}}$ **do**
4: $\quad \Psi = \mathbf{A}_{\mathrm{r}}^q\mathbf{R}_{\bar{y}\bar{y},m}\mathbf{W}_{\mathrm{res},m}$
5: $\quad n = \arg\max_{l=1,\ldots 2^{N_\phi+N_\theta}}(\Psi\Psi^H)_{l,l}$
6: $\quad \mathbf{W}_{\mathrm{RF},m} = [\mathbf{W}_{\mathrm{RF},m}|\mathbf{A}_{\mathrm{r}}^{q,n}]$
7: $\quad \mathbf{W}_{\mathrm{res},m} = [\,], \mathbf{W}_{\mathrm{BB},m} = [\,]$
8: $\quad$ **for** $k = 0 : K-1$ **do**
9: $\quad\quad \mathbf{W}_{\mathrm{BB},m}[k] = (\mathbf{W}_{\mathrm{RF},m}^H\mathbf{R}_{\bar{y}\bar{y},m}[k]\mathbf{W}_{\mathrm{RF},m})^{-1}$
$\quad\quad\quad \times \mathbf{W}_{\mathrm{RF},m}^H\mathbf{R}_{\bar{y}\bar{y},m}[k]\mathbf{W}_{\mathrm{MMSE},m}[k]$
10: $\quad\quad \mathbf{W}_{\mathrm{res},m}[k] = \dfrac{\mathbf{W}_{\mathrm{MMSE},m}[k]-\mathbf{W}_{\mathrm{RF},m}\mathbf{W}_{\mathrm{BB},m}[k]}{||\mathbf{W}_{\mathrm{MMSE},m}[k]-\mathbf{W}_{\mathrm{RF},m}\mathbf{W}_{\mathrm{BB},m}[k]||_F}$
11: $\quad\quad \mathbf{W}_{\mathrm{res},m} = \mathrm{blkdiag}(\mathbf{W}_{\mathrm{res},m}, \mathbf{W}_{\mathrm{res},m}[k])$
12: $\quad$ **end for** (k)
13: **end for** (i)
14: *return* $\mathbf{W}_{\mathrm{RF},m}, \mathbf{W}_{\mathrm{BB},m}$

With the aid of Eq. (26), the stage-1 hybrid TPC design problem can be mathematically written as

$$\min_{\mathbf{F}_{\mathrm{RF}},\{\mathbf{F}_{\mathrm{BB},m}^1[k]\}_{m,k=1}^{M,K}} \frac{1}{K}\sum_{k=1}^{K}\sum_{m=1}^{M}\left(N_{\mathrm{s}}\right.$$
$$\left. - \left\|(\mathbf{V}_m^{\mathrm{eff},1}[k])^H\mathbf{F}_{\mathrm{RF}}\mathbf{F}_{\mathrm{BB},m}^1[k]\right\|_F^2\right),$$
$$\text{s.t. } |\mathbf{F}_{\mathrm{RF}}(i,j)| = \frac{1}{\sqrt{N_{\mathrm{t}}}}, \forall i,j,$$
$$\mathbf{F}_{\mathrm{RF}}\{\mathbf{F}_{\mathrm{BB},m}^1[k]\}_{m,k=1}^{M,K} \in \mathcal{U}_{N_{\mathrm{t}}\times N_{\mathrm{s}}}. \quad (27)$$

Moreover, in a mmWave MIMO-OFDM system, the BB-TPCs for all the SUs on each subcarrier are updated in parallel. Therefore, one can eliminate the sum over m and k and can rewrite Eq.(27) as

$$(\mathbf{F}_{\mathrm{RF}}^{\mathrm{opt}}, \mathbf{F}_{\mathrm{BB}}^{1,\mathrm{opt}}) = \min_{\mathbf{F}_{\mathrm{RF}},\mathbf{F}_{\mathrm{BB}}^1}\left(KMN_{\mathrm{s}} - \left\|\mathbf{F}_{\mathrm{opt}}^H\mathbf{F}_{\mathrm{RF}}\mathbf{F}_{\mathrm{BB}}^1\right\|_F^2\right),$$
$$\text{s.t. } |\mathbf{F}_{\mathrm{RF}}(i,j)| = \frac{1}{\sqrt{N_{\mathrm{t}}}}, \forall i,j,$$
$$\mathbf{F}_{\mathrm{RF}}\mathbf{F}_{\mathrm{BB}}^1 \in \mathcal{U}_{N_{\mathrm{t}}\times KMN_{\mathrm{s}}}, \quad (28)$$

where $\mathbf{F}_{\mathrm{opt}} = [\mathbf{V}^{\mathrm{eff},1}[1],\ldots,\mathbf{V}^{\mathrm{eff},1}[k],\ldots,\mathbf{V}^{\mathrm{eff},1}[K]]$ and $\mathbf{V}^{\mathrm{eff},1}[k] = [\mathbf{V}_1^{\mathrm{eff},1}[k],\ldots,\mathbf{V}_m^{\mathrm{eff},1}[k],\ldots,\mathbf{V}_M^{\mathrm{eff},1}[k]]$. Similarly, $\mathbf{F}_{\mathrm{BB}}^1 = [\mathbf{F}_{\mathrm{BB}}^1[1],\ldots,\mathbf{F}_{\mathrm{BB}}^1[k],\ldots,\mathbf{F}_{\mathrm{BB}}^1[K]]$ and $\mathbf{F}_{\mathrm{BB}}^1[k] = [\mathbf{F}_{\mathrm{BB},1}^1[k],\ldots,\mathbf{F}_{\mathrm{BB},m}^1[k],\ldots,\mathbf{F}_{\mathrm{BB},M}^1[k]]$.

Due to the non-convex nature of the constant magnitude constraint on each element of the RF-TPC $\mathbf{F}_{\mathrm{RF}}$, the direct optimization of (28) is intractable. Several unique precoding solutions have been developed in response to this problem. In particular, the proposed SOMP based sparse precoding algorithm in [6] can also be applied to solve the problem in (28). However, the primary disadvantages of such a sparse hybrid design are the usage of quantized codebooks, which depend on the array geometry, and the associated correlation

operation used to generate the RF-TPC $\mathbf{F}_{\mathrm{RF}}$, which is computationally expensive. Additionally, the algorithm's accuracy depends on the angular resolution L, where $L = 2^{N_\phi + N_\theta}$, and (N_ϕ, N_θ) are the number of quantization bits pair utilized to quantify the azimuth and elevation angular ranges, respectively. In general, the goal is to solve the problem on a grid as fine as possible, i.e., with a very large value of L. Unfortunately, this results in a significantly increased computational complexity. As a first step in this direction, the authors in [39] propose a low-complexity hybrid TPC design procedure using the alternating minimization (HD-AM) principle, which eliminates the costly correlation operation otherwise required to calculate the RF-TPC $\mathbf{F}_{\mathrm{RF}}$, but is applicable only when $M_{\mathrm{t}} = N_{\mathrm{s}}$. For the scenario when $M_{\mathrm{t}} > N_{\mathrm{s}}$, the authors propose a finite unitary search technique for computation of the weights of the hybrid TPC that has lower complexity in comparison to the SOMP algorithm, but still depends on the array geometry. A new method of applying the HD-AM principle to the scenario when $M_{\mathrm{t}} > N_{\mathrm{s}}$ was recently proposed by the authors in [31]. In fact, this procedure can be modified to reduce the complexity further, while simultaneously improving performance, as will be seen later. Authors in [8] and [9] proposed different hybrid TPC design techniques considering constraints on the number of RF chains (M_{t}) and on the number of data streams (N_{s}). However, these designs are not invariant of M_{t} and N_{s}. Inspired by [8], this study proposes a novel alternative technique toward solving the aforementioned optimization problem, without necessitating any knowledge of the array geometry or limits on M_{t} and N_{s}. However, the condition $M_{\mathrm{t}} = N_{\mathrm{s}}$ can be considered as a special case of the proposed design. The various steps in the procedure proposed to solve the optimization problem in (28) are listed below:

1) To begin with, the solution for the BB-TPC $\mathbf{F}_{\mathrm{BB}}^1$ is derived in closed-form, for a fixed RF-TPC $\mathbf{F}_{\mathrm{RF}}$, which maximizes the overall SE in (24), without considering the MUI. The BB-TPC is thus obtained by solving the optimization problem in (28). Moreover, the $\mathbf{F}_{\mathrm{BB}}^1$ thus determined is constrained to be semi-unitary as can be seen from the constraint in (28).

2) Next, using the BB-TPC $\mathbf{F}_{\mathrm{BB}}^1$ as a starting point, we address the optimization problem (28) and devise an iterative approach to update the RF-TPC $\mathbf{F}_{\mathrm{RF}}$.

3) On completion of the last iteration of the procedure in the previous step, the BB-TPC $\mathbf{F}_{\mathrm{BB}}^1$ is modified using a least squares solution to further reduce the objective function.

4) In the second stage, the BB-TPC $\mathbf{F}_{\mathrm{BB}}^2[k] \forall k$ is designed using the zero-forcing (ZF) technique to mitigate the MUI.

We refer to this procedure as hybrid precoder design via modified alternating minimization-zeroforcing (MAM-ZF). The following subsection provides an in-depth examination of the various steps associated with this algorithm.

A. HYBRID TPC DESIGN

Given an RF-TPC $\mathbf{F}_{\mathrm{RF}}$, the procedure to calculate the BB-TPC weights is described in this part. From Eq. (26) it can be seen that the MUI term is decoupled from the design of the stage1 hybrid TPC $\mathbf{F}_{\mathrm{RF}}, \{\mathbf{F}_{\mathrm{BB},m}^1[k]\}_{m,k=1}^{M,K}$. Therefore, the problem below can be considered for designing the optimal stage1 BB-TPC for a given RF-TPC without loss of optimality

$$\max_{\{\mathbf{F}_{\mathrm{BB}}^1[k]\}_{k=1}^K} \frac{1}{K} \sum_{m=1}^M \sum_{k=1}^K \log_2 \left(\left| I_{N_{\mathrm{s}}} + \mathbf{R}_{\mathrm{n},m}^{-1}[k] \mathbf{H}_m^{\mathrm{eff}}[k] \right. \right.$$
$$\left. \left. \times \mathbf{F}_{\mathrm{RF}} \mathbf{F}_{\mathrm{BB},m}^1[k] (\mathbf{F}_{\mathrm{BB},m}^1[k])^H \mathbf{F}_{\mathrm{RF}}^H (\mathbf{H}_m^{\mathrm{eff}}[k])^H \right| \right)$$

$$\text{s.t..} \quad \mathbf{F}_{\mathrm{RF}} \{\mathbf{F}_{\mathrm{BB},m}^1[k]\}_{m,k=1}^{M,K} \in \mathcal{U}_{N_{\mathrm{t}} \times N_{\mathrm{s}}}. \quad (29)$$

Given the RF-TPC $\mathbf{F}_{\mathrm{RF}}$, the closed form solution for the above problem (29) can be obtained via the well-known water-filling principle [8], [24], which is given as

$$\{\mathbf{F}_{\mathrm{BB}}^1[k]\}_{k=1}^K = (\mathbf{F}_{\mathrm{RF}}^H \mathbf{F}_{\mathrm{RF}})^{-\frac{1}{2}} \{\widetilde{\mathbf{V}}[k]\}_{k=1}^K, \quad (30)$$

where $\widetilde{\mathbf{V}}[k] = [\widetilde{\mathbf{V}}_1[k], \dots, \widetilde{\mathbf{V}}_m[k], \dots, \widetilde{\mathbf{V}}_M[k]]$ and $\widetilde{\mathbf{V}}_m[k]$ is derived as follows. Considering the SVD of $\mathbf{H}_m^{\mathrm{eff}}[k]$ as given in Eq.(25), let the SVD of the matrix $\Sigma_m^{\mathrm{eff}}[k](\mathbf{V}_m^{\mathrm{eff}}[k])^H \mathbf{F}_{\mathrm{RF}}(\mathbf{F}_{\mathrm{RF}}^H \mathbf{F}_{\mathrm{RF}})^{-\frac{1}{2}}$ be computed as $\Sigma_m^{\mathrm{eff}}[k](\mathbf{V}_m^{\mathrm{eff}}[k])^H \mathbf{F}_{\mathrm{RF}}(\mathbf{F}_{\mathrm{RF}}^H \mathbf{F}_{\mathrm{RF}})^{-\frac{1}{2}} = \overline{\mathbf{U}}_m[k] \overline{\Sigma}_m[k] \overline{\mathbf{V}}_m^H[k]$. Then, the quantity $\widetilde{\mathbf{V}}_m[k] = \left[\overline{\mathbf{V}}_m[k] \right]_{:, 1:N_{\mathrm{s}}}$.

Now, by stacking $\mathbf{F}_{\mathrm{BB}}^1[k]$ and $\widetilde{\mathbf{V}}[k]$ for all subcarriers k, one can rewrite Eq.(30) as

$$\mathbf{F}_{\mathrm{BB}}^1 = (\mathbf{F}_{\mathrm{RF}}^H \mathbf{F}_{\mathrm{RF}})^{-\frac{1}{2}} \widetilde{\mathbf{V}}, \quad (31)$$

where $\widetilde{\mathbf{V}} = [\widetilde{\mathbf{V}}[1], \dots, \widetilde{\mathbf{V}}[k], \dots, \widetilde{\mathbf{V}}[K]]$ and $\mathbf{F}_{\mathrm{BB}}^1 = [\mathbf{F}_{\mathrm{BB}}^1[1], \dots, \mathbf{F}_{\mathrm{BB}}^1[k], \dots, \mathbf{F}_{\mathrm{BB}}^1[K]]$.

B. ANALOG PRECODER DESIGN

Our aim is now to design the RF-TPC $\mathbf{F}_{\mathrm{RF}}$, for the given BB-TPC $\mathbf{F}_{\mathrm{BB}}^1 = (\mathbf{F}_{\mathrm{RF}}^H \mathbf{F}_{\mathrm{RF}})^{-\frac{1}{2}} \widetilde{\mathbf{V}}$. On substituting the expression of $\mathbf{F}_{\mathrm{BB}}^1$ in the optimization problem (28), one can rewrite the optimization problem for $\mathbf{F}_{\mathrm{RF}}$ as

$$\mathbf{F}_{\mathrm{RF}}^{\mathrm{opt}} = \arg \min_{\mathbf{F}_{\mathrm{RF}}} \left(KMN_{\mathrm{s}} - \left\| \mathbf{F}_{\mathrm{opt}}^H \mathbf{F}_{\mathrm{RF}} (\mathbf{F}_{\mathrm{RF}}^H \mathbf{F}_{\mathrm{RF}})^{-\frac{1}{2}} \widetilde{\mathbf{V}} \right\|_F^2 \right),$$
$$\text{s.t.} \quad |\mathbf{F}_{\mathrm{RF}}(i,j)| = \frac{1}{\sqrt{N_{\mathrm{t}}}}, \forall i, j. \quad (32)$$

Note that, the above problem minimizes the average squared chordal distance between the two points $\mathbf{F}_{\mathrm{opt}}$ and $\mathbf{F}_{\mathrm{RF}}(\mathbf{F}_{\mathrm{RF}}^H \mathbf{F}_{\mathrm{RF}})^{-\frac{1}{2}} \widetilde{\mathbf{V}}$ on the Grassmann manifold. Therefore, one can rewrite the problem of (32) as

$$\mathbf{F}_{\mathrm{RF}}^{\mathrm{opt}} = \arg \min_{\mathbf{F}_{\mathrm{RF}}} \Phi_{\mathrm{chord}} \left(\mathbf{F}_{\mathrm{opt}}, \mathbf{F}_{\mathrm{RF}}(\mathbf{F}_{\mathrm{RF}}^H \mathbf{F}_{\mathrm{RF}})^{-\frac{1}{2}} \widetilde{\mathbf{V}} \right),$$
$$\text{s.t.} \quad |\mathbf{F}_{\mathrm{RF}}(i,j)| = \frac{1}{\sqrt{N_{\mathrm{t}}}}, \forall i, j. \quad (33)$$

As the chordal distance between two points on a Grassmann manifold is invariant under right multiplication of both of them by a semi-unitary matrix $\mathcal{U}_{N_t \times KMN_s}$, it follows that

$$\Phi_{\text{chord}}\left(\mathbf{F}_{\text{opt}}, \mathbf{F}_{\text{RF}}(\mathbf{F}_{\text{RF}}^H \mathbf{F}_{\text{RF}})^{-\frac{1}{2}} \widetilde{\mathbf{V}}\right)$$
$$= \Phi_{\text{chord}}\left(\mathbf{F}_{\text{opt}} \widetilde{\mathbf{V}}^H, \mathbf{F}_{\text{RF}}(\mathbf{F}_{\text{RF}}^H \mathbf{F}_{\text{RF}})^{-\frac{1}{2}}\right). \quad (34)$$

Given the $\mathbf{F}_{\text{RF}}$ per-entry constant modulus restriction, determining the exact solution to (33) is non-trivial. When no constraints are imposed on the elements of $\mathbf{F}_{\text{RF}}$, the solution to the above problem (33) is obtained by calculating the Karcher mean of the KM M_t-dimensional subspace formed by the points $\left\{\mathbf{V}_m^{\text{eff},1}[k] \widetilde{\mathbf{V}}_m^H[k]\right\}_{m,k=1}^{M,K}$, which can be mathematically expressed as [8]

$$\mathbf{F}_u^{\text{opt}} = \underset{\mathbf{F}_u \in \mathbb{C}^{N_t \times M_t}}{\arg\min} \Phi_{\text{chord}}\left(\mathbf{F}_{\text{opt}} \widetilde{\mathbf{V}}^H, \mathbf{F}_u\right),$$
$$= eig_{1:M_t}(\mathbf{F}_{\text{opt}} \widetilde{\mathbf{V}}^H (\mathbf{F}_{\text{opt}} \widetilde{\mathbf{V}}^H)^H), \quad (35)$$

where $eig_{1:M_t}(\mathbf{X})$ denotes the first M_t eigenvectors corresponding to the M_t largest eigenvalues. Note that, there is no constraint imposed on $\mathbf{F}_u$. Utilizing the triangle inequality for the chordal distance [40], the quantity $\Phi_{\text{chord}}\left(\mathbf{F}_{\text{opt}} \widetilde{\mathbf{V}}^H, \mathbf{F}_{\text{RF}}(\mathbf{F}_{\text{RF}}^H \mathbf{F}_{\text{RF}})^{-\frac{1}{2}}\right)$ can be upper-bounded as

$$\Phi_{\text{chord}}\left(\mathbf{F}_{\text{opt}} \widetilde{\mathbf{V}}^H, \mathbf{F}_{\text{RF}}(\mathbf{F}_{\text{RF}}^H \mathbf{F}_{\text{RF}})^{-\frac{1}{2}}\right)$$
$$- \Phi_{\text{chord}}\left(\mathbf{F}_{\text{opt}} \widetilde{\mathbf{V}}^H, \mathbf{F}_u\right) \le \Phi_{\text{chord}}\left(\mathbf{F}_u, \mathbf{F}_{\text{RF}}(\mathbf{F}_{\text{RF}}^H \mathbf{F}_{\text{RF}})^{-\frac{1}{2}}\right). \quad (36)$$

We consider the design of the RF-TPC $\mathbf{F}_{\text{RF}}$ such that it minimizes the upper bound given by Eq.(36). Therefore, the modified optimization problem for designing $\mathbf{F}_{\text{RF}}$ can be stated as

$$\mathbf{F}_{\text{RF}}^{\text{opt}} = \underset{\mathbf{F}_{\text{RF}}}{\arg\min} \Phi_{\text{chord}}\left(\mathbf{F}_u, \mathbf{F}_{\text{RF}}(\mathbf{F}_{\text{RF}}^H \mathbf{F}_{\text{RF}})^{-\frac{1}{2}}\right),$$
$$s.t. \ |\mathbf{F}_{\text{RF}}(i,j)| = \frac{1}{\sqrt{N_t}}, \forall i, j. \quad (37)$$

The above problem is still intractable due to the per entry constant magnitude constraint of $\mathbf{F}_{\text{RF}}$. To render the problem tractable, the following approximations are employed.

1) For frequency selective mmWave MIMO channels with a large number of antennas, the columns of $\mathbf{F}_{\text{RF}}$ can be configured to be nearly orthogonal, i.e, $(\mathbf{F}_{\text{RF}}^H \mathbf{F}_{\text{RF}}) \approx \mathbf{I}$.
2) The points $\mathbf{F}_u$ and $\mathbf{F}_{\text{RF}}(\mathbf{F}_{\text{RF}}^H \mathbf{F}_{\text{RF}})^{-\frac{1}{2}}$ can be made significantly close.

Consequently, utilizing the locally Euclidean property of the manifold, one can replace the chordal distance in Eq.(37) with the Euclidean distance, and the optimization problem for $\mathbf{F}_{\text{RF}}$ can be transformed to the following approximately equivalent problem

$$\mathbf{F}_{\text{RF}}^{\text{opt}} = \underset{\mathbf{F}_{\text{RF}}}{\arg\min} ||\mathbf{F}_u - \mathbf{F}_{\text{RF}}||_F^2,$$

$$s.t. \ |\mathbf{F}_{\text{RF}}(i,j)| = \frac{1}{\sqrt{N_t}}, \forall i, j. \quad (38)$$

Therefore, the RF-TPC design problem in (38) can now be converted to a per entry optimization problem for which the optimal solution is given by

$$\mathbf{F}_{\text{RF}} = \frac{1}{\sqrt{N_t}} e^{j \angle \mathbf{F}_u}. \quad (39)$$

The above Eq.(39) is being used as the update rule for the RF-TPC $\mathbf{F}_{\text{RF}}$ in each iteration, for a given BB-TPC $\mathbf{F}_{\text{BB}}^1$ obtained from Eq.(31). This iterative process to determine the BB-TPC $\mathbf{F}_{\text{BB}}^1$ and RF-TPC $\mathbf{F}_{\text{RF}}$ is now repeated till convergence. Furthermore, recall that the update rule for $\mathbf{F}_{\text{BB}}^1$ incorporates a semi-unitary constraint. To obtain a non semi-unitary solution for $\mathbf{F}_{\text{BB}}^1$, that further minimizes the optimization objective of (28), $\mathbf{F}_{\text{BB}}^1$ is updated using the least squares solution as $\mathbf{F}_{\text{BB}}^1 = (\mathbf{F}_{\text{RF}}^H \mathbf{F}_{\text{RF}})^{-1} \mathbf{F}_{\text{RF}}^H \mathbf{F}_{\text{opt}}$ after completion of the last iteration of the above algorithm. Following this, the stage-2 BB-TPCs $\left\{\mathbf{F}_{\text{BB}}^2[k]\right\}_{k=1}^K$ are constructed using a low-complexity ZF technique, the procedure for which is detailed in the subsequent subsection.

We now propose a modification to the HD-AM based precoding algorithm, described in [31], for a multiuser MIMO-OFDM system, in order to reduce the computational complexity and improve the performance. In particular we modify the initialization procedure for $\mathbf{F}_{\text{RF}}$. Irrespective of the BB-TPC ($\mathbf{F}_{\text{BB}}^1$), the RF-TPC ($\mathbf{F}_{\text{RF}}$) can be initialized such that the average distance between $\mathbf{F}_{\text{RF}}$ and optimal TPCs $\left\{\widetilde{\mathbf{V}}_m[k]\right\}_{m,k=1}^{M,K}$ is minimized, since the spatial and frequency-flat RF-TPC $\mathbf{F}_{\text{RF}}$ is being used by all the SUs for all subcarriers [41]. Therefore, by leveraging the manifold's locally Euclidean property, a sub-optimal solution for $\mathbf{F}_{\text{RF}}$ can be determined by solving the following problem

$$\mathbf{F}_{\text{RF}}^{\text{subopt}} = \underset{\mathbf{F}_{\text{RF}}}{\arg\min} ||\widetilde{\mathbf{F}}_u - \mathbf{F}_{\text{RF}}||_F^2,$$
$$s.t. \ |\mathbf{F}_{\text{RF}}(i,j)| = \frac{1}{\sqrt{N_t}}, \forall i, j, \quad (40)$$

where $\widetilde{\mathbf{F}}_u$ is given by

$$\widetilde{\mathbf{F}}_u = eig_{1:M_t} \mathbf{F}_{\text{opt}} \mathbf{F}_{\text{opt}}^H. \quad (41)$$

Similar to Eq. (38), the solution of Eq. (40) is given by

$$\mathbf{F}_{\text{RF}} = \frac{1}{\sqrt{N_t}} e^{j \angle \widetilde{\mathbf{F}}_u}. \quad (42)$$

The above solution can now be employed to initialize $\mathbf{F}_{\text{RF}}$. This reduces the number of iterations required for convergence, in comparison to the scheme in [31], in turn leading to a reduction in the computational complexity. This technique for hybrid precoding is referred to as low complexity alternating minimization-zeroforcing (LAM-ZF).

C. STAGE-2 BB PRECODING
Next, the stage-2 BB-TPC $\mathbf{F}_{\text{BB}}^2[k]$ is constructed to mitigate the MUI. We use the ZF approach to design $\left\{\mathbf{F}_{\text{BB}}^2[k]\right\}_{k=1}^K$

Algorithm 2 Hybrid Precoding via Modified Alternating Minimization-Zeroforcing (MAM-ZF) Technique at the CBS

Input: $\left\{\mathbf{H}_m^{\text{eff}}[k], \right\}_{m,k=1}^{M,K}$, $\mathbf{F}_{\text{opt}}$, N_1 (Number of iterations)

Output: $\mathbf{F}_{\text{RF}}, \left\{\mathbf{F}_{\text{BB}}[k]\right\}_{k=1}^{K}$

Initialization: $\mathbf{F}_{\text{RF}} = \mathbf{1}_{N_t \times M_t}$

for $n = 1, \ldots, N_1$ **do**
  1) Update $\mathbf{F}_{\text{BB}}^1$ using equation (31)
  2) Update $\mathbf{F}_{\text{RF}}$ by solving Eq.(32) whose solution is given by Eq.(39)
  end for
  3) Update $\mathbf{F}_{\text{BB}}^1$ as $\mathbf{F}_{\text{BB}}^1 = (\mathbf{F}_{\text{RF}}^H \mathbf{F}_{\text{RF}})^{-1} \mathbf{F}_{\text{RF}}^H \mathbf{F}_{\text{opt}}$
  4) Design $\mathbf{F}_{\text{BB}}^2[k]$, $\forall k$ using Eq.(43).
  5) Design $\mathbf{F}_{\text{BB}}[k]$ as $\mathbf{F}_{\text{BB}}[k] = [\mathbf{F}_{\text{BB},1}^1[k]\mathbf{F}_{\text{BB},1}^2[k], \ldots, \mathbf{F}_{\text{BB},M}^1[k]\mathbf{F}_{\text{BB},M}^2[k]]$, $\forall k$

Return: $\mathbf{F}_{\text{RF}}, \left\{\mathbf{F}_{\text{BB}}[k]\right\}_{k=1}^{K}$

Algorithm 3 Hybrid Precoding via Low Complexity Alternating Maximization-Zeroforcing (LAM-ZF) Technique at the CBS

Input: $\left\{\mathbf{H}_m^{\text{eff}}[k], \right\}_{m,k=1}^{M,K}$, $\mathbf{F}_{\text{opt}}$, N_2 (Number of iterations)

Output: $\mathbf{F}_{\text{RF}}, \left\{\mathbf{F}_{\text{BB}}[k]\right\}_{k=1}^{K}$

Initialization: $\mathbf{F}_{\text{RF}} = \frac{1}{\sqrt{N_t}} e^{j\angle \widetilde{\mathbf{F}}_u}$

for $n = 1, \ldots, N_2$ **do**
  1) Update $\mathbf{F}_{\text{BB}}^1$ as $\mathbf{F}_{\text{BB}}^1 = (\mathbf{F}_{\text{RF}}^H \mathbf{F}_{\text{RF}})^{-1} \mathbf{F}_{\text{RF}}^H \mathbf{F}_{\text{opt}}$
  2) Update the residue $\mathbf{F}_{\text{res}} = \mathbf{F}_{\text{opt}} - \mathbf{F}_{\text{RF}} \mathbf{F}_{\text{BB}}^1$
  3) Update $\mathbf{F}_{\text{RF}}$ as $\mathbf{F}_{\text{RF}} = \frac{1}{\sqrt{N_t}} e^{j\angle (\mathbf{F}_{\text{res}}(\mathbf{F}_{\text{BB}}^1)^H + \mathbf{F}_{\text{RF}})}$
  end for
  4) Update $\mathbf{F}_{\text{BB}}^1$ as $\mathbf{F}_{\text{BB}}^1 = (\mathbf{F}_{\text{RF}}^H \mathbf{F}_{\text{RF}})^{-1} \mathbf{F}_{\text{RF}}^H \mathbf{F}_{\text{opt}}$
  5) Design $\mathbf{F}_{\text{BB}}^2[k]$, $\forall k$ using Eq.(43).
  6) Design $\mathbf{F}_{\text{BB}}[k]$ as $\mathbf{F}_{\text{BB}}[k] = [\mathbf{F}_{\text{BB},1}^1[k]\mathbf{F}_{\text{BB},1}^2[k], \ldots, \mathbf{F}_{\text{BB},M}^1[k]\mathbf{F}_{\text{BB},M}^2[k]]$, $\forall k$

Return: $\mathbf{F}_{\text{RF}}, \left\{\mathbf{F}_{\text{BB}}[k]\right\}_{k=1}^{K}$

---

in order to reduce the design complexity. In this scheme, the CBS computes the effective channel as $\left\{\widetilde{\mathbf{H}}_m^{\text{eff}}[k]\right\}_{m,k=1}^{M,K} = \left\{\mathbf{H}_m^{\text{eff}}[k]\mathbf{F}_{\text{RF}}\mathbf{F}_{\text{BB},m}^1[k]\right\}_{m,k=1}^{M,K} \in \mathbb{C}^{N_s \times N_s}$, and concatenates them as $\left\{\bar{\mathbf{H}}[k]\right\}_{k=1}^{K} = \left\{\left[\widetilde{\mathbf{H}}_1^{\text{eff}^T}[k] \ldots \widetilde{\mathbf{H}}_M^{\text{eff}^T}[k]\right]^T\right\}_{k=1}^{K} \in \mathbb{C}^{MN_s \times N_s}$. Subsequently, the ZF-BB-TPC $\left\{\mathbf{F}_{\text{BB}}^2[k]\right\}_{k=1}^{K}$ is designed as

$$\left\{\mathbf{F}_{\text{BB}}^2[k]\right\}_{k=1}^{K} = \left\{(\bar{\mathbf{H}}^H[k]\mathbf{H}[\bar{\mathbf{k}}])^{-1}\bar{\mathbf{H}}^H[k]\right\}_{k=1}^{K}. \quad (43)$$

Therefore, the final BB-TPC at the kth subcarrier can be written as $\mathbf{F}_{\text{BB}}[k] = [\mathbf{F}_{\text{BB},1}^1[k]\mathbf{F}_{\text{BB},1}^2[k], \ldots, \mathbf{F}_{\text{BB},M}^1[k]\mathbf{F}_{\text{BB},M}^2[k]]$. The overall design procedure of the proposed MAM-ZF technique is given in Algorithm 2 whereas the steps in LAM-ZF algorithm are succinctly described in Algorithm 3.

D. OPTIMAL POWER LOADING
Note that, with the aid of $\mathbf{F}_{\text{BB},m}^2[k]$, the interference-plus-noise covariance $\mathbf{R}_{\text{in},m}[k]$ closely approaches the noise covariance $\mathbf{R}_{\text{n},m}[k]$ since the interference covariance $\mathbf{R}_{\text{i},m}[k] \to \mathbf{0}$. Therefore, using Eq. (26), the optimal power loading vector $\mathbf{p}[k] \forall k$ can now be calculated by solving the optimization problem below

$$\mathbf{p}^{\text{opt}}[k] = \max_{\{\mathbf{p}_m[k]\}_{m=1}^{M}} \sum_{m=1}^{M} \log_2 \left(\left|I_{N_s} + (\mathbf{F}_{\text{BB},m}^2[k])^H \right.\right.$$
$$\times (\Sigma_m^{\text{eff},1}[k])^H (\mathbf{U}_m^{\text{eff}}[k])^H \mathbf{R}_{\text{n},m}^{-1}[k]\mathbf{U}_m^{\text{eff}}[k]\Sigma_m^{\text{eff},1}[k]\mathbf{F}_{\text{BB},m}^2[k]$$
$$\left.\left.\times \text{diag}(\mathbf{p}_m[k])\right|\right)$$
$$s.t.\ J_0[k] \le I_{\text{th}},$$
$$\left|\left|\mathbf{F}_{\text{RF}}\mathbf{F}_{\text{BB}}[k]\text{diag}(\sqrt{\mathbf{p}[k]})\right|\right|_F^2 \le P_{\text{max}}. \quad (44)$$

Let us denote the dth diagonal element of $\text{diag}(\mathbf{p}_m[k])$ as $p_{m,d}[k]$, which corresponds to the optimal power allocated to

dth stream of the mth SU on a particular subcarrier k. Then, by following the well-known water-filling algorithm [30], [42], the closed-form solution for $p_{m,d}[k]$ can be determined as

$$p_{m,d}[k]$$
$$= \max \left\{0, \frac{1}{\lambda\zeta_{m,d}[k] + \omega t_{m,d}[k]} - \frac{\sigma^2}{\gamma_{m,d}^2[k]\|\mathbf{f}_{\text{BB},m}^{2,(d)}[k]\|^2}\right\}$$
$$\forall k, m, d, \quad (45)$$

where $\zeta_{m,d}[k]$, $t_{m,d}[k]$ and $\gamma_{m,d}^2[k]$ denote the dth diagonal elements of $\left(\mathbf{F}_{BB,m}^H[k]\mathbf{F}_{\text{RF}}^H\mathbf{G}^H[k]\mathbf{G}[k]\mathbf{F}_{\text{RF}}\mathbf{F}_{BB,m}[k]\right)$, $\left(\mathbf{F}_{BB,m}^H[k]\mathbf{F}_{\text{RF}}^H\mathbf{F}_{\text{RF}}\mathbf{F}_{BB,m}[k]\right)$ and $\Sigma_m^{\text{eff},1}[k]$, respectively. Furthermore, $\mathbf{f}_{\text{BB},m}^{2,(d)}[k]$ represents the dth column of $\mathbf{F}_{\text{BB},m}^2[k]$, while λ and ω are the Lagrange multipliers associated with the first and the second constraints, respectively, of the problem in Eq. (44).

V. COMPLEXITY ANALYSIS
In this section, we comprehensively analyze the computational complexity of the proposed hybrid TPC/RC design and compare it to existing schemes. We evaluate the complexity of each step in the design algorithm by computing the total number of floating-point operations (FLOPs) involved in the worst case scenario. It is important to highlight that a complex multiplication operation carries a higher computational cost compared to a complex addition operation. However, for calculation purposes, we treat each operation, whether it is complex multiplication or complex addition, as one FLOP. Consider a codebook of resolution $\mathcal{O}(G_r)$ at each SU for the MSOMP-based hybrid-RC design algorithm, and a codebook

TABLE 2. Complexity comparison of proposed algorithm with extensions of other existing algorithms from literature.

Method	Complexity
Hybrid-TPC design via SOMP [6]	$\mathcal{O}(G_t N_t M_t K M N_s)$
Hybrid-TPC design of [31]	$\mathcal{O}(N_t M_t K M N_s N_3)$ [1]
Proposed MAM-ZF-based hybrid-TPC design	$\mathcal{O}(M_t^2 K M N_s N_1)$
Proposed LAM-ZF-based hybrid-TPC design	$\mathcal{O}(N_t M_t K M N_s N_2)$

[1]We consider, N_3 is the number of iteration used in the TPC algorithm proposed in [31].

resolution of $\mathcal{O}(G_t)$ at the CBS for the SOMP-based TPC design algorithm. Table 2 below presents a comparative analysis of the complexity of the proposed TPC design in relation to other existing approaches from the literature, considering their extension to the present system model. Table 2 illustrates that the proposed precoding technique, MAM-ZF, exhibits a lower complexity in comparison to the other precoding methods. Furthermore, as explained in Section IV, it is always true that $N_2 < N_3$. As a result, the complexity of the proposed LAM-ZF-based precoding technique is lower than that of the algorithm described in [31].

VI. SIMULATION RESULTS

This section presents simulation results to demonstrate the efficacy of the proposed frequency selective blind hybrid MMSE-RC solution presented in Section(III), followed by the proposed two-stage decoupled strategy for hybrid TPC design and optimal power loading solutions presented in Section(IV). The performance obtained is compared with that of the LAM-ZF based design, the greedy SOMP based design of [6], as well as benchmarked with respect to the conventional fully digital beamformer. The wideband mmWave MIMO channel is generated as specified in (5)-(8), where the pulse shaping function $p_{rc}(t)$ is considered to be a raised-cosine filter. Therefore, $p_{rc}(t)$ is modeled as

$$p_{rc}(t) = \begin{cases} \dfrac{\pi}{4}\mathrm{sinc}(\dfrac{1}{2\beta}), & t = \pm\dfrac{T_s}{2\beta} \\ \mathrm{sinc}(\dfrac{t}{T_s})\dfrac{cos(\dfrac{\pi\beta t}{T_s})}{1-(\dfrac{2\beta t}{T_s})^2}, & \text{otherwise,} \end{cases} \quad (46)$$

where T_s is the sampling time and β represents the roll-of factor which is set to unity. For each $N_{tap} = 3$ delay-tap channel (5), the propagation environment is modelled as a $N_{cl} = 8$ cluster environment with $N_p = 10$ multi-path components per cluster. The complex gain of the lth path in the cth scattering cluster, denoted by $\alpha_{cl,m} \forall m$, is generated as an i.i.d. sample of a $\mathcal{CN}(\mathbf{0}, \sigma^2_{\alpha,c,m})$ random variable. In each cluster, the N_p azimuth and elevation AoD/AoA pairs $(\phi^t_{cl,m}, \theta^t_{cl,m})/(\phi^r_{cl,m}, \theta^r_{cl,m})$ are generated from a truncated Laplacian distribution with uniformly-random mean cluster angle of $(\phi^t_{c,m}, \theta^t_{c,m})/(\phi^r_{c,m}, \theta^r_{c,m})$ and a constant angular spread of $(\sigma_{\phi^t}, \sigma_{\theta^t})/(\sigma_{\phi^r}, \sigma_{\theta^r})$, respectively. For simplicity, we assume $\sigma_{\phi^t} = \sigma_{\theta^t} = \sigma_{\phi^r} = \sigma_{\theta^r} = \sigma_c = \frac{1}{\sqrt{2}}$. Moreover, the transmitter and receiver antenna elements are considered to be ideal sectoral elements with unit gain over the sector defined by $[\phi_{min}, \phi_{max}]$ in the azimuth domain and $[\theta_{min}, \theta_{max}]$ in the elevation domain [6], [43]. The

TABLE 3. Simulation parameters.

Parameter	value
System dimension ($N_r \times N_t$)	8×128 and 16×256
Number of cluster (N_{cl})	8
Number of multi-path (N_p)	10
Number of delay taps (N_{tap})	3
Pulse shaping function ($p_{rc}(t)$)	raised-cosine (46)
Roll-of factor (β)	1
Carrier frequency F_s	70 GHz
Transmitter sector azimuth $[\phi^t_{min}, \phi^t_{max}]$	$[-30°, 30°]$
Transmitter sector elevation $[\theta^t_{min}, \theta^t_{max}]$	$[80°, 100°]$
Receiver sector azimuth $[\phi^r_{min}, \phi^r_{max}]$	$[-180°, 180°]$
Receiver sector elevation	$[0°, 180°]$
Number of parallel stream per subcarrier (N_s)	2 and 4
Number of SU (M)	4
Number of RF chain at each SU (M_r)	$2N_s$
Number of RF chain at CBS (M_t)	MM_r
Number of subcarrier (K)	64
Per-subcarrier interference threshold (I_{th})	-15dB to 25dB
Per-subcarrier power budget (P_{max})	I_{th}
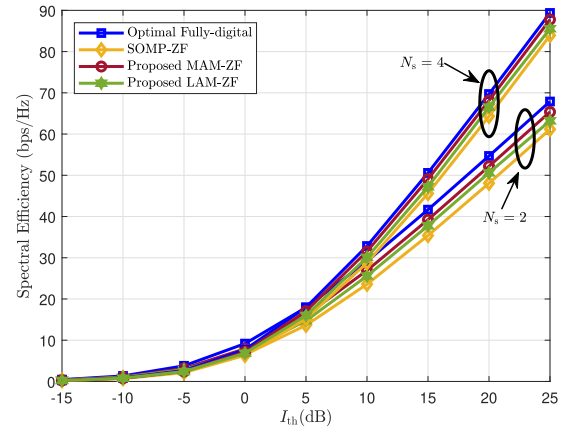
FIGURE 2. SE comparison among several TPC/RC design algorithms for a 8×128 mmWave MSU MIMO-OFDM CRN with $M = 4$, $M_r = 2N_s$, $M_t = MM_r$, and $K = 64$.

transmitter's sector azimuth is assumed to lie in the interval $[-30°, 30°]$ while the sector elevation is generated in the range $[80°, 100°]$. In contrast, we assume omni-directional users, i.e., the receiver sector azimuth and elevation lie in the intervals $[-180°, 180°]$, $[0°, 180°]$, respectively. While implementing the MSOMP algorithm described in Alg. [1] for hybrid MMSE RC design, each SU uses the quantized codebook given by Eq. (22), where $N_\phi = N_\theta = 3$ are being considered for calculation of $\mathbf{W}_{RF,m}$. Furthermore, the number of RF chains at the CBS is considered as $M_t = MM_r$, while the number of RF chains at each SU is set as $M_r = 2N_s$, similar to existing works [9], [24]. The per-subcarrier interference threshold is assumed to be constant and is set between -15dB to 25dB, and the per-subcarrier power budget, denoted by P_{max}, is set equal to I_{th}. All of the presented simulation findings are generated by averaging over 2000 random realizations of the mmWave MIMO-OFDM channel. Below, we have now listed the simulation parameters in Table 3 for ready reference.

Fig. 2 plots the SE realised by an 8×128 mmWave MSU MIMO-OFDM CRN, where a CBS with $N_t = 128$ antennas serves $M = 4$ SUs, each with $N_r = 8$ antennas, in the presence of a single PU. Fig. 3 plots the same for a
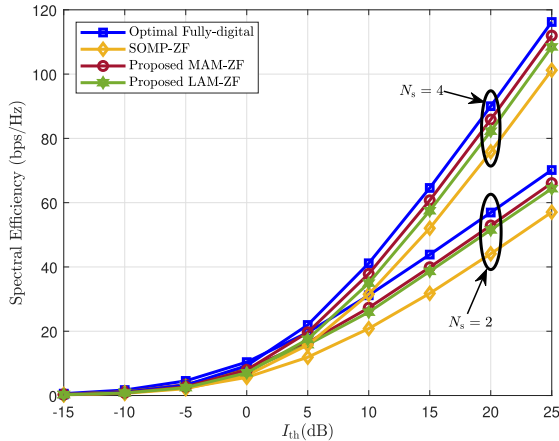
FIGURE 3. SE comparison among several TPC/RC design algorithms for a 16×256 mmWave MSU MIMO-OFDM CRN with $M = 4, M_r = 2N_s, M_t = MM_r$, and $K = 64$.

16×256 mmWave MSU MIMO-OFDM CRN. On each subcarrier, the number of per SU data streams is set as $N_s = 2$ and 4, which implies $M_r = 4$ and 8 and $M_t = 16$ and 32, respectively. From both the figures, it can be readily observed that the proposed MAM-ZF based precoding solution achieves the SE, which is close to the same achieved by the optimal FD-TPC/RC solution for both $N_s = 2$ and 4. The LAM-ZF based TPC solution appears to surpass the performance of SOMP-based precoding in terms of the overall performance. Therefore, in comparison to the LAM-ZF and SOMP-based precoding solutions, the proposed MAM-ZF based precoding solution can efficiently approximate the dominant singular vectors of the effective channel with a high degree of precision.

The requirement of number of RF chains for signal processing holds great significance, especially in the mmWave band, due to the substantial impact it has on the increased power consumption and hardware costs. To assess the effectiveness of our proposed algorithm in relation to the number of RF chains used, Fig.4 plots the SE performance attained by a 16×256 system with varying numbers of RF chains. In particular, the simulation parameters are set as $M = 4$, $N_s = 4$, $M_r = 4, 8, 12$ at each SU and $M_t = 16, 32, 48$ at the CBS. Fig.4(a) compares the performance achieved by MAM-ZF based precoding with that of its SOMP-based counterpart, and Fig.4(b) plots the same for LAM-ZF and SOMP-based precoding. From Fig.4(a) and 4(b), it can be readily observed that for all RF chain settings, the MAM-ZF and LAM-ZF precoding schemes perform better than SOMP-based precoding, which implies that both the MAM-ZF and LAM-ZF schemes have a higher power efficiency than the state-of-the-art SOMP based precoding scheme. Furthermore, when going from $M_r = N_s = 4$ to $M_r = 2N_s = 8$, there is a noticeable improvement in the SE performance compared to the increase of M_r from 8 to 12. This finding demonstrates that while $M_r \geq N_s$ is required in the hybrid architecture to realise fully-digital beamforming, $M_r \geq 2N_s$ is sufficient to achieve the best performance. It is crucial to note that

SOMP-based precoding with $M_r = 12$ performs worse than the proposed MAM-ZF based precoding with $M_r = 8$, as seen in Fig.4(a), which reinforces the poor performance of the former. Finally, Fig.4(c) plots the performance comparison between MAM-ZF and LAM-ZF precoding schemes for a varying number of RF chains. Note that, when $M_r = N_s$, there is a slight gap between the SE performance achieved by the MAM-ZF and LAM-ZF precoders, but when M_r increases beyond $2N_s$, i.e., $M_r = 12$ in this particular case, the improvement in the SE performance of LAM-ZF based precoding is negligible whereas that of the MAM-ZF approaches the ideal fully-digital scheme. Moreover, for all settings of M_r, the proposed MAM-ZF based precoding outperforms the LAM-ZF scheme. For illustration, at $I_{th} = 10$ dB, with $M_r = 4$, the SEs of the proposed MAM-ZF, LAM-ZF and SOMP-ZF based precoding respectively approach 71%, 69% and 58% of that reached by the optimal fully digital scheme, while with $M_r = 8$ the SEs reach approximately 92%, 87% and 79% of the fully digital performance, respectively.

With regard to practical deployments of wideband MSU-MIMO CRNs, the number of per-SU data streams on each subcarrier, i.e., N_s, as well as the number of SUs supported by the CBS, i.e., M, are two important parameters of the system. This is due to the fact that as the number of parallel data streams per subcarrier increases, the severity of inter-symbol interference (ISI) increases, and as the number of served SUs increases, the severity of multiuser interference (MUI) increases, both of which can potentially lead to a degradation in the performance of the system. To investigate this aspect, we examine the system performance by varying the multiplexing settings, i.e., by varying N_s and M, as depicted in Fig. 5 and Fig. 6, respectively. Fig. 5 plots the SE performance attained by different precoding schemes when N_s varies from 2 to 8, whereas Fig. 6 plots the same by varying M from 2 to 14, for three different PU-prescribed interference settings, viz., $I_{th} = \{5, 10, 15\}$ dB. The other parameters are $N_r = 16, N_t = 256, K = 64, M = 4$ for Fig. 5 and $N_r = 16, N_t = 256, K = 64, N_s = 4$ in Fig. 6. The number of RF chains at each SU set is set as $M_r = 2N_s$ and the number of RF chains at the CBS is set as $M_t = MM_r$. It can be seen from Fig. 5 that as N_s increases, the achievable SE initially increases to reach its peak, and subsequently decreases. The initial increment can be attributed to the increased number of MIMO spatial modes, characterized by the non-zero diagonal elements in $\Sigma_m^{eff}[k]$ for the mth SU at subcarrier K. However, with the increase in N_s, the effect of ISI becomes dominant, due to which the SE performance marginally decreases. Note that when $I_{th} = 15$ dB, the SE performance degrades after $N_s = 7$ streams per subcarrier, whereas for $I_{th} = 10$ dB and $I_{th} = 5$ dB, it begins degrading beyond $N_s = 5$ and 4 streams per subcarrier, respectively. This can be attributed to the fact that lower I_{th} leads to higher inter symbol interference. Furthermore, it is worth noting that in all cases considered in Fig. 5, the proposed MAM-ZF based precoding performs better than its
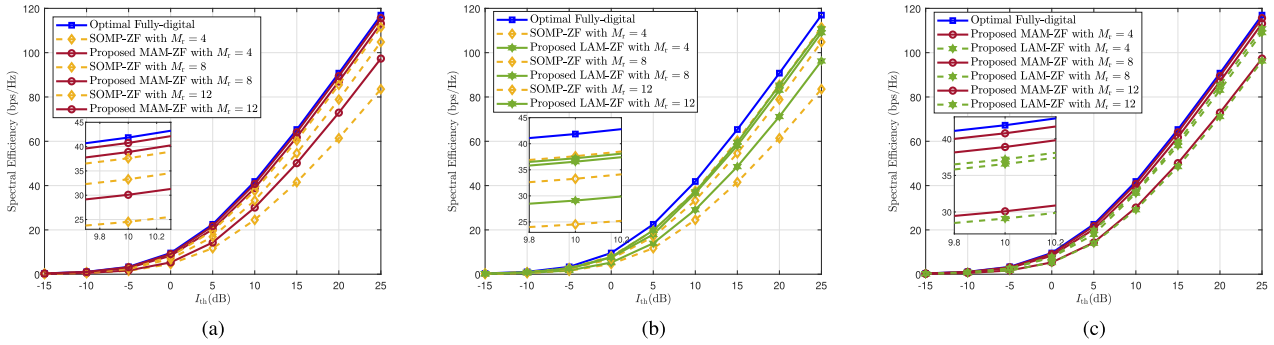
FIGURE 4. SE attained by varying M_r in (a) SOMP-ZF Vs. MAM-ZF (b) SOMP-ZF Vs. LAM-ZF (c) MAM-ZF Vs. LAM-ZF.
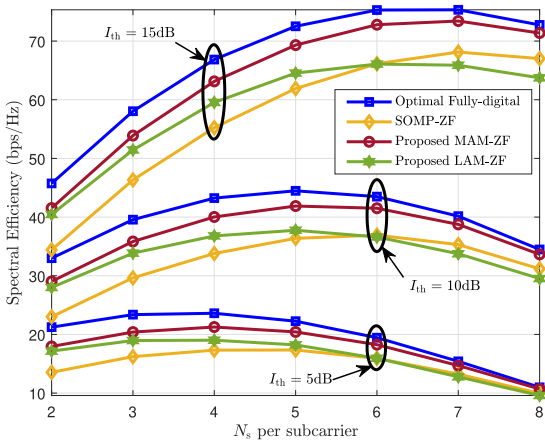

FIGURE 5. SE realised by various TPC/RC design algorithms in a 16×256 mmWave MSU MIMO-OFDM CRN where N_s varies from 2 to 8, $I_{th} = \{5, 10, 15\}$ dB, $K = 64$ and $M = 4$.
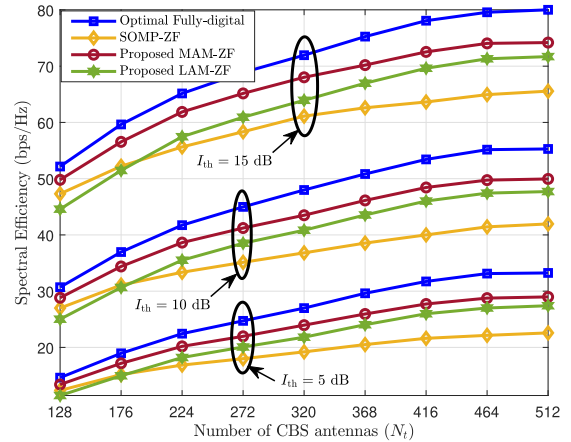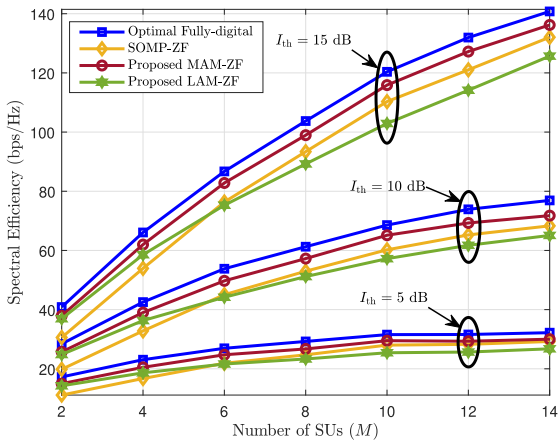

FIGURE 7. SE realised by various TPC/RC design algorithms in a 16×256 mmWave MSU MIMO-OFDM CRN where N_t varies from 128 to 512, $I_{th} = \{5, 10, 15\}$ dB, $M = N_s = 4$ and $K = 64$.
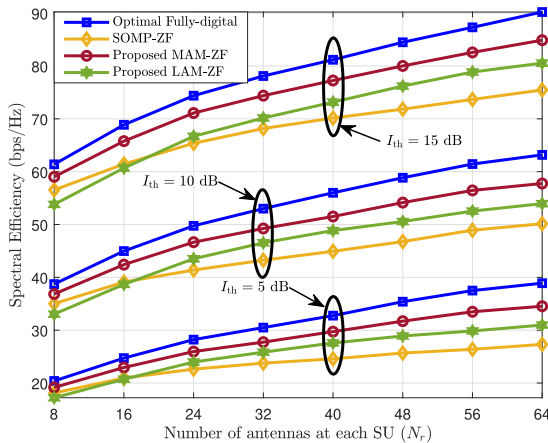

FIGURE 6. SE realised by various TPC/RC design algorithms in a 16×256 mmWave MSU MIMO-OFDM CRN where M varies from 2 to 14, $I_{th} = \{5, 10, 15\}$ dB, $K = 64$, and $N_s = 4$.

the proposed stage-2 ZF-BB-TPC $\left\{ \mathbf{F}_{BB}^2[k] \right\}_{k=1}^{K}$ in cancelling the MUI. Note that, in both Fig. 5 and Fig. 6, the LAM-ZF based precoding performs poorly in comparison to SOMP-ZF beyond $N_s = 6$ and $M = 6$, respectively. This is because, for a fixed K when either N_s increases or M increases, the number of columns in $\mathbf{F}_{opt}$ increases, which enhances the correlation between columns of $\mathbf{F}_{opt}$ when $KMN_s > N_t$, and introduces inter-symbol interference and MUI in the Karcher mean based solution of $\mathbf{F}_{RF}$ in (39). It can also be seen from Fig. 5 that when $N_s = 6$, which results in $KMN_s = 1536$, and when $M = 6$ in Fig. 6, which also leads $KMN_s = 1536$, the effect of inter-symbol interference and MUI becomes significant leading it to have a poor performance in comparison to SOMP.

Fig. 7 depicts the SE attained by the various TPC/RC solutions at three different interference settings, $I_{th} = \{5, 10, 15\}$ dB, when N_t increases from 128 to 512 for a fixed $N_r = 16$. Fig. 8 displays the same by increasing N_r from 8 to 64 while keeping N_t at 256. The other parameters are set as $M = N_s = 4$, $K = 64$, $M_r = 2N_s$ and $M_t = MM_r$. It can be readily observed from both the figures that as the number of CBS antennas N_t or the number of SU antennas N_r increases, the SE of the various precoding schemes improves. This is because higher number of transmit and receive antennas leads to narrow beams, which enhances the transmit/receive

LAM-ZF and SOMP-based precoding counterparts. Fig. 6 shows that the SEs achieved by all the different precoding schemes continue to rise as the number of SUs, M increases, with the proposed MAM-ZF based precoding outperforming the same achieved by LAM-ZF and SOMP-based precoding. It is important to emphasize that we consider the same ZF based MUI cancellation technique for all the precoding schemes. The continuous increment in the SE performance for increasing values of M demonstrates the effectiveness of

FIGURE 8. SE realised by various TPC/RC design algorithms in a 16×256 mmWave MSU MIMO-OFDM CRN where N_r varies from 8 to 64, $I_{th} = \{5, 10, 15\}$ dB, $M = N_s = 4$ and $K = 64$.

beamforming gain. Moreover, the proposed MAM-ZF based precoding shows a considerable performance gain when compared to the LAM-ZF and SOMP-ZF algorithms for the same, for all values of I_{th}. In addition, note that as N_t increases, the performance gain of the proposed techniques over the SOMP-ZF design also improves. However, note that, compared with a system that has a small number of antennas at the CBS and SU, the performance gap between the proposed beamforming scheme and the optimal fully digital scheme is larger. Based on these results, it appears that increasing the number of CBS antennas or SU antennas can improve the SE without requiring additional power-intensive RF chains.

VII. CONCLUSION

Frequency-selective hybrid RC and TPC designs were proposed for a mmWave MSU-MIMO-OFDM downlink CRN to maximize the SE of SU transmission while restricting the interference introduced to the PU to lie within a specified threshold. Initially, the RC design problem was formulated and solved using the MSOMP technique to achieve MSE minimization. Next, a two-step TPC design strategy was proposed, which comprised of a novel alternating minimization-based technique for the stage-1 TPC design and a ZF-based technique for the stage-2 BB-TPC design. Following this, the solution for the optimal power loading scheme was derived in closed-form to satisfy the interference and transmit power budget constraints while simultaneously maximizing the spectral efficiency of the CRN. Results obtained from computer simulations showed that, compared to existing techniques, the proposed schemes are capable of achieving a SE close to that of ideal fully-digital beamforming with a much fewer number of RF chains.

REFERENCES

[1] A. Ghosh, T. A. Thomas, M. C. Cudak, R. Ratasuk, P. Moorut, F. W. Vook, T. S. Rappaport, G. R. MacCartney, S. Sun, and S. Nie, "Millimeter-wave enhanced local area systems: A high-data-rate approach for future wireless networks," *IEEE J. Sel. Areas Commun.*, vol. 32, no. 6, pp. 1152–1163, Jun. 2014.

[2] I. A. Hemadeh, K. Satyanarayana, M. El-Hajjar, and L. Hanzo, "Millimeter-wave communications: Physical channel models, design considerations, antenna constructions, and link-budget," *IEEE Commun. Surveys Tuts.*, vol. 20, no. 2, pp. 870–913, 2nd Quart., 2018.

[3] I. F. Akyildiz, W.-Y. Lee, M. C. Vuran, and S. Mohanty, "A survey on spectrum management in cognitive radio networks," *IEEE Commun. Mag.*, vol. 46, no. 4, pp. 40–48, Apr. 2008.

[4] A. Goldsmith, S. A. Jafar, I. Maric, and S. Srinivasa, "Breaking spectrum gridlock with cognitive radios: An information theoretic perspective," *Proc. IEEE*, vol. 97, no. 5, pp. 894–914, May 2009.

[5] A. Sharmila and P. Dananjayan, "Spectrum sharing techniques in cognitive radio networks—A survey," in *Proc. IEEE Int. Conf. Syst., Comput., Autom. Netw. (ICSCAN)*, Mar. 2019, pp. 1–4.

[6] O. E. Ayach, S. Rajagopal, S. Abu-Surra, Z. Pi, and R. W. Heath Jr., "Spatially sparse precoding in millimeter wave MIMO systems," *IEEE Trans. Wireless Commun.*, vol. 13, no. 3, pp. 1499–1513, Mar. 2014.

[7] X. Gao, L. Dai, S. Han, I. Chih-Lin, and R. W. Heath Jr., "Energy-efficient hybrid analog and digital precoding for mmWave MIMO systems with large antenna arrays," *IEEE J. Sel. Areas Commun.*, vol. 34, no. 4, pp. 998–1009, Apr. 2016.

[8] A. Alkhateeb and R. W. Heath Jr., "Frequency selective hybrid precoding for limited feedback millimeter wave systems," *IEEE Trans. Commun.*, vol. 64, no. 5, pp. 1801–1818, May 2016.

[9] F. Sohrabi and W. Yu, "Hybrid analog and digital beamforming for mmWave OFDM large-scale antenna arrays," *IEEE J. Sel. Areas Commun.*, vol. 35, no. 7, pp. 1432–1443, Jul. 2017.

[10] A. K. Gupta, J. G. Andrews, and R. W. Heath Jr., "On the feasibility of sharing spectrum licenses in mmWave cellular systems," *IEEE Trans. Commun.*, vol. 64, no. 9, pp. 3981–3995, Sep. 2016.

[11] M. Rebato, F. Boccardi, M. Mezzavilla, S. Rangan, and M. Zorzi, "Hybrid spectrum sharing in mmWave cellular networks," *IEEE Trans. Cognit. Commun. Netw.*, vol. 3, no. 2, pp. 155–168, Jun. 2017.

[12] H. S. Ghadikolaei, H. Ghauch, G. Fodor, M. Skoglund, and C. Fischione, "A hybrid model-based and data-driven approach to spectrum sharing in mmWave cellular networks," *IEEE Trans. Cognit. Commun. Netw.*, vol. 6, no. 4, pp. 1269–1282, Dec. 2020.

[13] G. Li, T. Irnich, and C. Shi, "Coordination context-based spectrum sharing for 5G millimeter-wave networks," in *Proc. 9th Int. Conf. Cognit. Radio Oriented Wireless Netw. Commun. (CROWNCOM)*, Jun. 2014, pp. 32–38.

[14] H. Shokri-Ghadikolaei, F. Boccardi, C. Fischione, G. Fodor, and M. Zorzi, "Spectrum sharing in mmWave cellular networks via cell association, coordination, and beamforming," *IEEE J. Sel. Areas Commun.*, vol. 34, no. 11, pp. 2902–2917, Nov. 2016.

[15] C. Vrontos, F. Boccardi, S. Armour, E. Mellios, and J. Butler, "Performance evaluation of spectrum sharing in mmWave cellular networks using ray-tracing," in *Proc. IEEE Wireless Commun. Netw. Conf. (WCNC)*, May 2020, pp. 1–6.

[16] P. K. Sangdeh, H. Pirayesh, A. Quadri, and H. Zeng, "A practical spectrum sharing scheme for cognitive radio networks: Design and experiments," *IEEE/ACM Trans. Netw.*, vol. 28, no. 4, pp. 1818–1831, Aug. 2020.

[17] M. G. Khoshkholgh, K. Navaie, and H. Yanikomeroglu, "Interference management in underlay spectrum sharing using indirect power control signalling," *IEEE Trans. Wireless Commun.*, vol. 12, no. 7, pp. 3264–3277, Jul. 2013.

[18] S. Park, A. Alkhateeb, and R. W. Heath Jr., "Dynamic subarrays for hybrid precoding in wideband mmWave MIMO systems," *IEEE Trans. Wireless Commun.*, vol. 16, no. 5, pp. 2907–2920, May 2017.

[19] K. B. Dsouza, K. N. R. S. V. Prasad, and V. K. Bhargava, "Hybrid precoding with partially connected structure for millimeter wave massive MIMO OFDM: A parallel framework and feasibility analysis," *IEEE Trans. Wireless Commun.*, vol. 17, no. 12, pp. 8108–8122, Dec. 2018.

[20] H. Yuan, J. An, N. Yang, K. Yang, and T. Q. Duong, "Low complexity hybrid precoding for multiuser millimeter wave systems over frequency selective channels," *IEEE Trans. Veh. Technol.*, vol. 68, no. 1, pp. 983–987, Jan. 2019.

[21] T.-H. Tsai, M.-C. Chiu, and C.-C. Chao, "Sub-system SVD hybrid beamforming design for millimeter wave multi-carrier systems," *IEEE Trans. Wireless Commun.*, vol. 18, no. 1, pp. 518–531, Jan. 2019.

[22] J. Du, W. Xu, C. Zhao, and L. Vandendorpe, "Weighted spectral efficiency optimization for hybrid beamforming in multiuser massive MIMO-OFDM systems," *IEEE Trans. Veh. Technol.*, vol. 68, no. 10, pp. 9698–9712, Oct. 2019.

[23] G. M. Zilli and W.-P. Zhu, "Constrained tensor decomposition-based hybrid beamforming for mmWave massive MIMO-OFDM communication systems," *IEEE Trans. Veh. Technol.*, vol. 70, no. 6, pp. 5775–5788, Jun. 2021.

[24] F. Sohrabi and W. Yu, "Hybrid digital and analog beamforming design for large-scale antenna arrays," *IEEE J. Sel. Topics Signal Process.*, vol. 10, no. 3, pp. 501–513, Apr. 2016.

[25] C. G. Tsinos, S. Maleki, S. Chatzinotas, and B. Ottersten, "Hybrid analog-digital transceiver designs for cognitive radio millimiter wave systems," in *Proc. 50th Asilomar Conf. Signals, Syst. Comput.*, 2016, pp. 1785–1789, doi: 10.1109/ACSSC.2016.7869690.

[26] M. Á. Vázquez, L. Blanco, and A. I. Pérez-Neira, "Hybrid analog–digital transmit beamforming for spectrum sharing backhaul networks," *IEEE Trans. Signal Process.*, vol. 66, no. 9, pp. 2273–2285, May 2018.

[27] L. Xu, L. Sun, G. Xia, T. Liu, F. Shu, Y. Zhang, and J. Wang, "Secure hybrid digital and analog precoder for mmWave systems with low-resolution DACs and finite-quantized phase shifters," *IEEE Access*, vol. 7, pp. 109763–109775, 2019.

[28] Z. Kong, J. Song, C. Wang, H. Chen, and L. Hanzo, "Hybrid analog-digital precoder design for securing cognitive millimeter wave networks," *IEEE Trans. Inf. Forensics Security*, vol. 16, pp. 4019–4034, 2021.

[29] C. G. Tsinos, S. Chatzinotas, and B. Ottersten, "Hybrid analog-digital transceiver designs for multi-user MIMO mmWave cognitive radio systems," *IEEE Trans. Cognit. Commun. Netw.*, vol. 6, no. 1, pp. 310–324, Mar. 2020.

[30] J. Singh, I. Chatterjee, S. Srivastava, A. Agrahari, A. K. Jagannatham, and L. Hanzo, "Hybrid transceiver design and optimal power allocation for the cognitive mmWave multiuser MIMO downlink relying on limited feedback," *IEEE Open J. Veh. Technol.*, vol. 4, pp. 241–256, 2023.

[31] M. Alouzi, F. Chan, and C. D'Amours, "Low complexity hybrid precoding and combining for millimeter wave systems," *IEEE Access*, vol. 9, pp. 95911–95924, 2021.

[32] A. Forenza, D. J. Love, and R. W. Heath Jr., "Simplified spatial correlation models for clustered MIMO channels with different array configurations," *IEEE Trans. Veh. Technol.*, vol. 56, no. 4, pp. 1924–1934, Jul. 2007.

[33] A. A. M. Saleh and R. Valenzuela, "A statistical model for indoor multipath propagation," *IEEE J. Sel. Areas Commun.*, vol. SAC-5, no. 2, pp. 128–137, Feb. 1987.

[34] J. W. Wallace and M. A. Jensen, "Statistical characteristics of measured MIMO wireless channel data and comparison to conventional models," in *Proc. IEEE 54th Veh. Technol. Conf. (VTC Fall)*, vol. 2, Oct. 2001, pp. 1078–1082.

[35] *Spatial Channel Model, SCM-134 Text V6. 0*, document, GTS Group, Spatial Channel Model AHG (Combined Ad-Hoc From 3GPP and 3GPP2), 2003.

[36] O. Famoriji, Z. Zhang, A. Fadamiro, R. Zakariyya, and F. Lin, "Planar array diagnostic tool for millimeter-wave wireless communication systems," *Electronics*, vol. 7, no. 12, p. 383, Dec. 2018. [Online]. Available: https://www.mdpi.com/2079-9292/7/12/383

[37] C. A. Balanis, "Antenna theory: A review," *Proc. IEEE*, vol. 80, no. 1, pp. 7–23, Jan. 1992.

[38] S. Kay, *Fundamentals of Statistical Signal Processing: Detection Theory* (Fundamentals of Statistical Si). Upper Saddle River, NJ, USA: Prentice-Hall, 1998. [Online]. Available: https://books.google.co.in/books?id=vA9LAQAAIAAJ

[39] A. Alkhateeb, G. Leus, and R. W. Heath Jr., "Limited feedback hybrid precoding for multi-user millimeter wave systems," *IEEE Trans. Wireless Commun.*, vol. 14, no. 11, pp. 6481–6494, Nov. 2015.

[40] R.-A. Pitaval, O. Tirkkonen, and S. D. Blostein, "Density and bounds for Grassmannian codes with chordal distance," in *Proc. IEEE Int. Symp. Inf. Theory*, Jul. 2011, pp. 2298–2302.

[41] J. Singh, I. Chatterjee, S. Srivastava, and A. K. Jagannatham, "Hybrid transceiver design and optimal power allocation in downlink mmWave hybrid MIMO cognitive radio systems," in *Proc. Nat. Conf. Commun. (NCC)*, May 2022, pp. 178–183.

[42] G. Bansal, M. Hossain, and V. Bhargava, "Optimal and suboptimal power allocation schemes for OFDM-based cognitive radio systems," *IEEE Trans. Wireless Commun.*, vol. 7, no. 11, pp. 4710–4718, Nov. 2008.

[43] S. Singh, R. Mudumbai, and U. Madhow, "Interference analysis for highly directional 60-GHz mesh networks: The case for rethinking medium access control," *IEEE/ACM Trans. Netw.*, vol. 19, no. 5, pp. 1513–1527, Oct. 2011.

INDRANIL CHATTERJEE received the B.Tech. degree in electronics and communication engineering (ECE) from Techno Main Salt Lake, India, in 2018. He is currently pursuing the M.S. degree in electrical engineering (EE) with the Indian Institute of Technology Kanpur, Kanpur, India, specializing in signal processing, communication, and networks (SPCOM). His research interests include physical layer design of 5G wireless systems, cognitive radio systems, and mmWave communications.
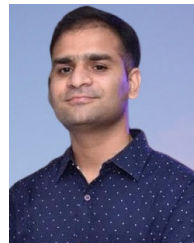
JITENDRA SINGH (Member, IEEE) received the integrated dual B.Tech. and M.Tech. degrees in electronics and communication engineering with specialization in wireless communication and networks from Gautam Buddha University, Greater Noida, India, in 2017. He is currently pursuing the Ph.D. degree with the Department of Electrical Engineering, Indian Institute of Technology Kanpur, Kanpur, India. His research interests include cognitive radio networks, mmWave communication, intelligent reflecting surface (IRS), and integrated sensing and communication (ISAC) systems.

SURAJ SRIVASTAVA (Member, IEEE) received the M.Tech. degree in electronics and communication engineering from the Indian Institute of Technology Roorkee, India, in 2012, and the Ph.D. degree in electrical engineering from the Indian Institute of Technology Kanpur, Kanpur, India, in 2022. From July 2012 to November 2013, he was a Staff-I Systems Design Engineer with Broadcom India Private Ltd., Bengaluru. From November 2013 to December 2015, he was a Lead Engineer with Samsung Research India, Bengaluru, where he worked on developing layer-2 of the 3G UMTS/WCDMA/HSDPA modem. His research interests include applications of sparse signal processing in 5G wireless systems, mmWave and terahertz communication, orthogonal time-frequency space (OTFS), joint radar and communication (RadCom), and optimization and machine learning. He was awarded the Outstanding Ph.D. Thesis and the Outstanding Teaching Assistant Awards from the IIT Kanpur. He was awarded the Qualcomm Innovation Fellowship (QIF) from Qualcomm, in 2018 and 2022.

ADITYA K. JAGANNATHAM (Senior Member, IEEE) received the bachelor's degree from the Indian Institute of Technology Bombay, and the M.S. and Ph.D. degrees from the University of California at San Diego, San Diego, CA, USA. From April 2007 to May 2009, he was a Senior Wireless Systems Engineer with Qualcomm Inc., San Diego, where he was a part of the Qualcomm CDMA Technologies (QCT) Division. He is currently a Professor with the Department of Electrical Engineering, IIT Kanpur, where he also holds the Arun Kumar Chair Professorship. His research interests include next-generation wireless cellular and WiFi networks, with a special emphasis on various 5G technologies, and such as massive MIMO, mmWave MIMO, FBMC, NOMA, and full duplex. He has been twice awarded the P. K. Kelkar Young Faculty Research Fellowship for excellence in research, the Qualcomm Innovation Fellowship (QInF), the IIT Kanpur Excellence in Teaching Award, the CAL(IT)2 Fellowship from the University of California at San Diego, and the Upendra Patel Achievement Award from Qualcomm.

• • •